Mineralium Deposita
https://doi.org/10.1007/s00126-024-01282-3

ARTICLE

Petrogenesis of Ni-sulfide mineralisation in the ca. 3.0 Ga Maniitsoq intrusive belt, western Greenland

Wolfgang D. Maier[1] · D. D. Muir[1] · S-. J. Barnes[2] · K. Szilas[3]

Received: 15 January 2024 / Accepted: 9 May 2024

Abstract

The ca. 3.0 Ga Ni sulfide mineralisation at Maniitsoq, SW Greenland, is hosted by a cluster of relatively small, irregularly shaped mafic-ultramafic intrusions, typically 10s of m to a few km across, that are lodged within broadly coeval gneiss. Many of the intrusions are fault bounded and fragmented so that their original sizes remain unknown. The sulfides form disseminations and sulfide matrix breccia veins displaying sharp contacts to the host intrusives. The mineralisation has relatively high Ni/Cu, with 4–10% Ni and 1–2% Cu. Correlations between Ni and Cu with sulfide content are strong, consistent with a magmatic origin of the mineralisation. PGE contents are mostly below 0.5 ppm, and Cu/Pd is typically above primitive mantle levels, interpreted to reflect equilibration of the parent magma with segregating sulfide melt prior to final magma emplacement. Sulfide segregation was likely triggered by assimilation of crustal sulfur, as suggested by whole rock S/Se ratios of 7000–9000. The sulfide melt underwent extensive fractionation after final emplacement, caused by downward percolation of Cu-rich sulfide melt through incompletely solidified cumulates. We suggest that the exposed Maniitsoq intrusions represent the Ni-rich upper portions of magma conduits implying that there is potential for Cu-rich sulfides in unexposed deeper portions of the belt.

Keywords Nickel sulfides · Archean ore deposits · Greenland · Magma conduit

Introduction

Numerous sulfide-mineralised, predominantly mafic intrusives occur in the vicinity of the village of Maniitsoq (pop. 2500), SW Greenland, ~100–150 km to the north of Nuuk (Fig. 1). More than 30 mineralised bodies have so far been identified, within an exploration licence area of ~3000 km^2. The property is accessible year-round by boat from Nuuk or Maniitsoq, as a result of the Irminger and West Greenland currents, which bring warm water from the Gulf Stream northwards along the southwest coast of Greenland. The intrusions have previously been grouped into the so-called "Greenland Norite Belt" (Nielsen 1976; Secher 1983; Garde et al. 2013), extending for ~75 km in N-S, and 15 km in E-W direction. However, we will show in the following that most rocks in the belt contain significant clinopyroxene, i.e. are gabbronorites. True norites make up a smaller proportion, and pyroxenite and diorite are relatively rare (see also Waterton et al. 2020). It is possible if not likely that the pre-metamorphic mineral assemblage contained relatively less clinopyroxene, with relatively more calcic plagioclase. However, in order to reduce terminological ambiguity and to highlight the economic potential of the area, we will use the term "Maniitsoq Nickel Belt" for the studied intrusions.

The Maniitsoq project area is underlain by the North Atlantic Craton. In western Greenland, the craton comprises six shear zone-bounded blocks, exposing granulite facies rocks in the north and prograde amphibolite facies rocks in the south (Windley and Garde 2009). From south to north, the blocks are: Ivittuut, Kvanefjord, Bjørnesund, Sermilik, Fiskefjord, and Maniitsoq. The Ni-bearing intrusions are hosted within the Fiskefjord block (Fig. 1A). It

Editorial handling: E. Mansur.

✉ Wolfgang D. Maier
maierw@cardiff.ac.uk

[1] School of Earth and Environmental Sciences, Cardiff University, Cardiff, UK

[2] Sciences de la Terre, Université du Québec à Chicoutimi, Chicoutimi, Canada

[3] Department of Geosciences and Natural Resource Management, University of Copenhagen, Copenhagen, Denmark

Published online: 13 June 2024

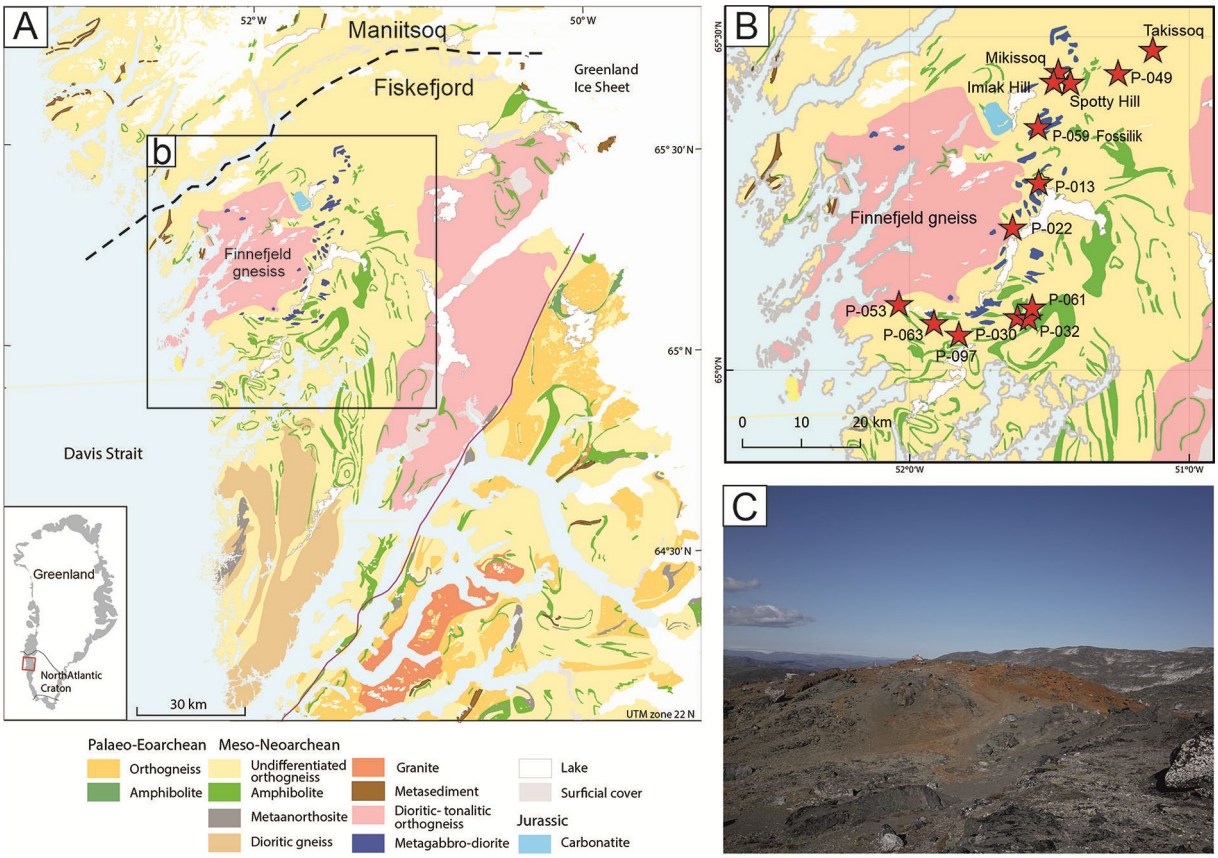

Fig. 1 **a**: Locality map (from Linnebjerg 2019). (**b**) Close-up showing localities of studied intrusions. (**c**) View of Imiak Hill gossan (from Linnebjerg 2019)

is separated from the Sermilik block by the structurally complex northeast-trending Godthåbsfjord-Ameralik Belt, which comprises several terranes of different ages that have been accreted tectonically and folded together (Windley and Garde 2009).

The dominant lithologies in the Fiskefjord block comprise supracrustal rocks intruded by multiple phases of felsic to ultramafic intrusions and dikes. Most rocks are Archean in age, with the exception of Proterozoic mafic dikes and a Paleozoic carbonatite. The ages of the main tonalite-trondhjemite-granodiorite (TTG) gneisses are between approximately 3,050 and 3,010 Ma, although there are also older (ca. 3.2 Ga) diorites in the southern part of the Fiskefjord block (Windley and Garde 2009; Olierook et al. 2021). The TTG gneisses are cut by younger intrusions including the Taserssuaq tonalite-granodiorite dated at 2,982 ± 7 Ma, the Qugssuk granite dated at 2,975 ± 6 Ma, and the Finnefjeld gneiss dated at 2,975 ± 7 Ma (Fig. 1, Garde et al. 2000). The latter forms a complex body of predominantly tonalitic and trondhjemitic rocks thought to have been emplaced after the main granulite facies metamorphic event (Windley and Garde 2009). The Finnefjeld gneiss is interpreted as a late-orogenic, deep-crustal, intrusive granitoid pluton (Allaart et al. 1978; Marker and Garde 1988) or alternatively as a deeply eroded impact structure (Garde et al. 2014). The TTG gneisses are embedded with kilometre-scale suites of mafic volcanic rocks (amphibolite) and enderbitic gneisses.

The Maniitsoq Ni belt consists of a group of tens of metre- to kilometre-scale mafic intrusions to the S and E of the Finnefjeld gneiss, forming a J-shaped belt approximately 75 km long and up to 15 km wide (Fig. 1B). The age of the intrusions varies between 3,014.0 +/- 2.7 Ma and 3,002.3 +/-5.4 Ma (Heaman 2014). A series of Proterozoic high-magnesium mafic dikes crosscutting the area are dated at ca. 2214 ± 10 Ma (Nutman et al. 1995).

Supracrustal lithological units in the belt include paragneiss, biotite schist, and amphibolite. Locally, the paragneisses contain several percent pyrite and pyrrhotite, e.g. in the northwestern portion of the belt, at the Takissoq West target (Fig. 1B), where sulfide mineralisation with elevated Cu and Zn levels was intersected during drilling. Voluminous paragneiss units, especially in the southern portion of the belt suggest the presence of a large metamorphosed sedimentary basin. The ages of paragneiss and amphibolite sequences are currently unknown, but most predate the ca. 3.0 Ga tonalitic orthogneiss.

The Maniitsoq intrusive belt has been explored for Ni-Cu sulfides since 1959, first by Kryolitselskabet Øresund A/S Company (KØ) and then by a range of other companies including Falconbridge, Nunaoil, Cominco, Planitonva, Monopros and IceFire Diamonds. From 1959 to 1973, KØ discovered many of the currently known nickel-copper sulfide occurrences. Peak grades of 8.40% Ni (at 0.07% Cu and 0.19% Co) were identified in an ultramafic rock at site 1965-41, along the SE edge of the licence area. North American Nickel (NAN) started exploration in 2012. Their activities focussed on testing for extensions of mineralisation at nine targets (Mikissoq, Imiak Hill, Spotty Hill, Fossilik, P-058, P-059, P-004, P-013, P-053 and P-030 and P-032). In 2019, NAN changed its name to Premium Nickel Resources Limited.

The sulfide mineralisation is almost invariably hosted by mafic-ultramafic bodies consisting of gabbronorite, norite, pyroxenite and diorite. The bodies are of highly irregular shape, forming pod-like and lenticular intrusions that can be up to 4 km^2 in surface extension. Less commonly, the bodies occur as metre-scale dikes. In the larger bodies, layering may occur due to varying pyroxene content (Secher 1982, Waterton et al. 2020).

The aim of this paper is to devise a petrogenetic model for the Ni sulfide mineralisation. This relies on detailed descriptions of the intrusions, including examination of several drill cores, mapping of microtextures, and interpretation of a large database of metal assays and whole rock silicate compositions. Maniitsoq constitutes one of the oldest Ni sulfide deposits on the planet, and we need to understand whether mid-Archean ore forming processes were substantially different from more recent settings.

Methods

Petrography

A petrographic description of sulfide-poor regional samples of the Maniitsoq Ni belt was published by Waterton et al. (2020). In the present study, we add information obtained by transmitted and reflected light microscopy on the Spotty Hill South ultramafic body.

Chemical mapping

High-resolution element maps were generated using a Carl Zeiss Sigma HD Analytical Field Emission Gun Scanning Electron Microscope (FEG-SEM) equipped with two Oxford Instruments X-MaxN 150 mm2 energy dispersive spectrometers (EDS) at Cardiff University. The maps were produced using an accelerating voltage of 20 kV, a 120 µm final aperture, with a nominal beam current of 4 nA and a working distance of 8.9 mm. For entire sections, a step size of 15–20 µm and a pixel dwell time of 10 ms was used. Corrections were applied to acquired maps for background removal, peak overlaps, and pulse pile-ups before being exported in AZtec 6.0 software.

Mineral compositional data

To complement the mineral compositional data of Waterton et al. (2020), in the present study we analysed orthopyroxene, clinopyroxene, plagioclase and olivine from the Spotty Hill South body, by quantitative EDS using the Cardiff SEM facility. A beam energy of 20 kV was used with a 60 µm final aperture with a nominal beam current of 1.5 nA and a working distance of 8.9 mm. Using a process time of 1 µs resulted in output count rates of 130,000 cps with a dead time of 50%. A livetime of 15 s resulted in almost 2 million counts per spectrum. Beam measurements were performed using pure cobalt and a range of microanalytical standards from Astimex Ltd and the Smithsonian were used to calibrate and assess relative accuracy for each element of interest on secondary standards.

Drill core assays

North American Nickel generated whole rock data on nearly 2000 drill core samples from the Maniitsoq Ni belt. Samples were analysed at a range of independent certified commercial laboratories, including Activation Laboratories Ltd. (Actlabs) in Ancaster, Ontario, ALS Global in North Vancouver, British Columbia, SGS Canada Inc. in Burnaby, British Colombia, and MS Analytical in Langley, British Columbia. Drill core samples were assayed for Ni, Cu, Co, Pt, Pd, Au and S as well as selected other major and/or trace elements. Analyses for Ni, Cu, Co and S and other selected elements were performed either by 4 acid digestion (2011, 2012, 2013, and 2014) or by sodium peroxide fusion and HCl dissolution (2015 and 2016) with an ICP-AES/OES (inductively coupled plasma optical emission spectrometry) finish. Analyses for Pt, Pd, and Au were performed by fire assay using a 30 g charge with an ICP-AES/OES or ICP-MS (mass spectroscopy) finish. Whole rock analyses were performed by borate fusion and ICP-AES and ICP-MS finishes. Detection limits are typically 2.5 ppb for Pt and Pd, 1 ppb for Au, and 5ppm for Ni and Cu.

Commercial certified reference materials (with a range of Ni, Cu, Co, Pt, Pd, and Au contents) and sample blanks were inserted in every batch of 20 core samples or a minimum of one per sample batch. Certified reference materials were sourced from CF Reference Materials Inc. of Sudbury, Ontario (CFRM-XX), Ore Research and Exploration Pty

Ltd. of Melbourne, Australia, Analytical Solutions Ltd of Mulmur, Ontario (OREAS-XX), and African Mineral Standards of Johannesburg, South Africa (AMIS-XX). Sample handling and preparation procedures and those used by the independent certified laboratories contracted by North American Nickel were reviewed by SRK (Ravenelle and Weyerhaeuser 2017). Overall, SRK considers that the analytical results delivered by the primary laboratories used by North American Nickel are reliable and do not present obvious evidence of analytical bias.

High-precision whole rock analysis of six sulfide-rich samples was performed at LabMaTer, Université du Québec à Chicoutimi. Most major and trace elements were determined by laser ablation-inductively coupled plasma-mass spectrometry (LA-ICP-MS) of a Li-tetraborate bead which contained 0.5 g of sample and 2.25 g of flux powder. The LA-ICP-MS analyses of the glass disks were performed using an Excimer 193 nm RESOlution M-50 laser ablation system (Australian Scientific Instrument) equipped with a double volume cell S-155 (Laurin Technic) and coupled with an Agilent 7900 mass spectrometer. Data reduction was carried out using the Iolite package for Igor Pro software (Paton et al. 2011). The isotopes measured for each element are reported in ESM 1. Calibration was carried out using a combination of S-rich reference materials (CCU-1, WMS-1a, PTC-1) and an in-house reference material which is a mixture of KPT-1 (Sudbury diabase) and NIST 610 in the ratio 10:1. This combination allowed calibration and matrix-matching for our S-rich samples. Silicate reference materials NIST 610, GeoPt18/KPT-1 (Sudbury diabase) and GeoPt 36 (a gabbro) were also used to monitor the results. The results obtained for the reference materials agree with the working values (ESM 1).

To determine Te, As, Bi, Sb and Se, the samples were dissolved following the technique described by Mansur et al. (2020b). The solutions were then analysed by two different methods, Hydride Generation Atomic Fluorescence Spectrometry (HG-AFS) and ICP-MS (Agilent 7700 mass spectrometer). Results for Te, As and Bi for international reference materials by HG-AFS show better agreement with working values than ICP-MS results. However, the concentrations of Se and Sb in the samples were higher than saturation levels for HG-AFS method and the ICP-MS results were used for these elements.

Platinum-group elements (Os, Ir, Ru, Rh, Pt, Pd) and Au were collected from 15 g of sample material using Ni sulfide fire assay, followed by dissolution in aqua regia. The concentrations were determined by ICP-MS (Agilent 7700 mass spectrometer) using the method described by Savard et al. (2010). Sulfur was determined by combustion and infrared analysis using a HORIBA EMIA-220 V analyser using the method described by Bédard et al. (2008). International reference materials OKUM, GeoPT-18/KPT-1 and WMS1a agree within error with certificate values (ESM 1).

Results

Drill core observations

In the following section we present drill core observations on five intrusions in the Maniitsoq Ni belt, namely Imiak Hill, Mikissoq (Imiak North), Spotty Hill, Fossilik and Central (Fig. 1B).

The main mineralised intervals measure typically several meters to locally 10s of meters in width and consist of sulfide-matrix breccias which display sharp contacts with the fine- or medium grained mafic host rock (Figs. 2 and 3). The breccia fragments mostly consist of norite, gabbronorite and pyroxenite, but amphibolite and gneiss locally also occur (Fig. 3I). The fragments are angular (Fig. 2B) or rounded (Fig. 2C, D,E). Most of the sulfides are pyrrhotite (po) with additional pentlandite (pn), pyrite (py) and chalcopyrite (ccp). The latter is highly irregularly distributed; In many samples it is rare, but may locally form the bulk of the sulfides (Fig. 2B). In places, host rock fragments appear to be partially dislodged by sulfide (Fig. 2D) seemingly invading the host rock in a downhole direction (Fig. 2E). In some of the intrusions, sulfide-matrix breccias are rare. Instead there are thick intervals of disseminated sulfides (Fig. 3A, B) forming isolated grains (Fig. 3A), clouds (Fig. 3B) or globules of interstitial sulfides (Fig. 3G). In addition to breccia veins and disseminated sulfides, there are numerous mm-sized sulfide veinlets, some of which are clearly fracture controlled (Fig. 3D, I). Veinlets consist of pyrrhotite, pentlandite, pyrite and chalcopyrite. In some cases, vein sulfide is associated with quartz (Fig. 3E).

Petrography and mineral compositions

The rocks of the Maniitsoq Ni belt are predominantly noritic and gabbronoritic, with less abundant pyroxenite, melanorite and leucogabbronorite. The rocks consist primarily of orthopyroxene, clinopyroxene, plagioclase, and hornblende with subordinate biotite, quartz and opaque minerals. Pyroxenes typically show partial to extensive replacement by hornblende ± biotite as a result of retrograde metamorphism (Windley and Garde 2009). Olivine-rich rocks are rare, except for an approximately 300 × 600 m, predominantly pyroxenitic body immediately to the south of Spotty Hill, mapped by Burden (2014) and Duncalf (2014). This body is termed Spotty Hill South here (Fig. 4, ESM 2). It has relatively low sulfide contents (up to 5% in OC43) and, unusually, the sulfide assemblage is markedly more

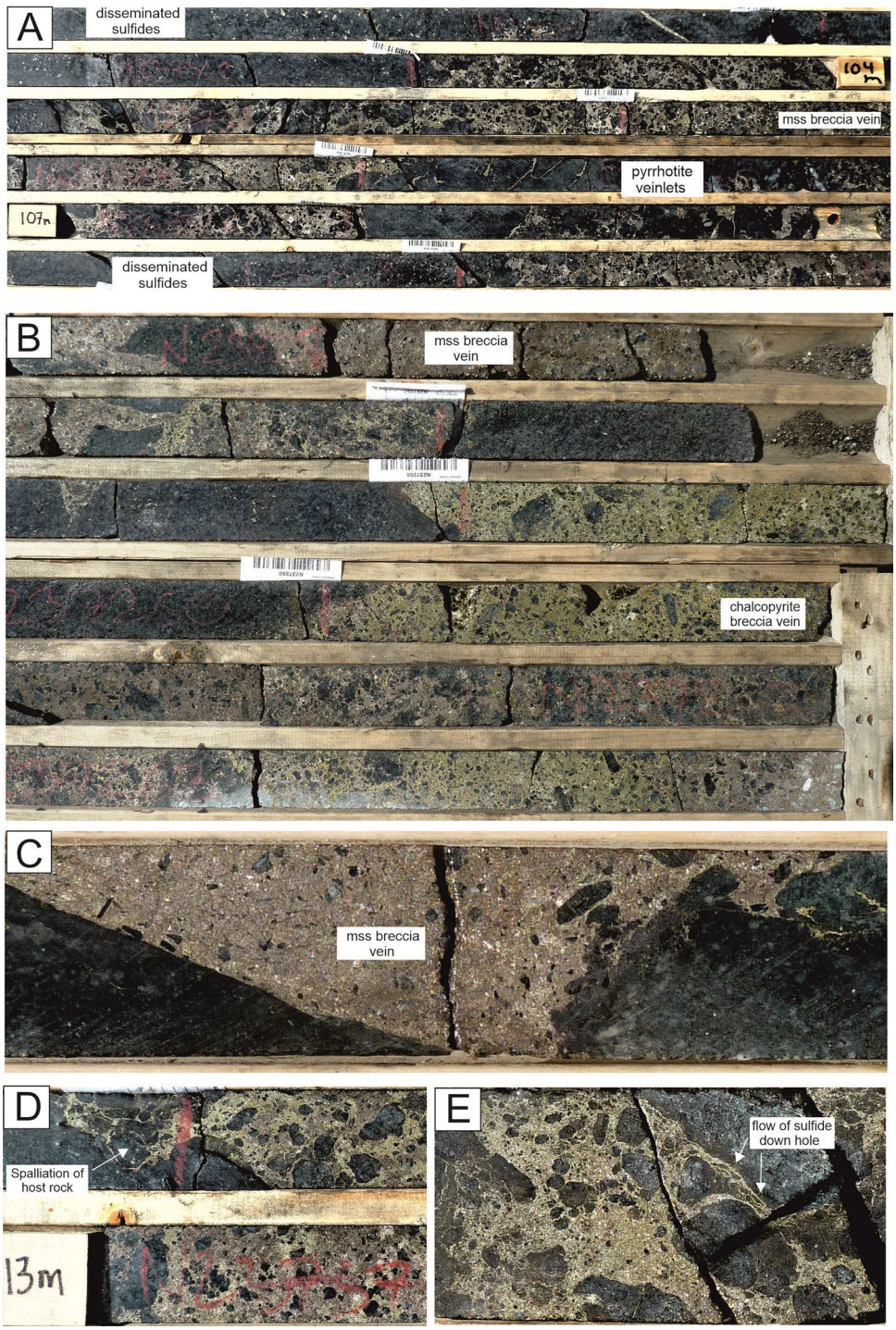

Fig. 2 (**A**) Mineralised interval at Mikissoq (MQ13-29), showing thick (m-scale) veins of sulfide matrix breccia as well as disseminated and vein sulfides in mafic silicate matrix. Note mostly sharp boundaries between breccia veins and mafic host rock, which has 14–15% MgO and 1000 ppm Cr. (**B**) Chalcopyrite-rich breccia vein at Imiak Hill (MQ13-28, 195.14–197.5 m) containing 4.5% Cu, 1.3–3.2% Ni, virtually zero PGE and Au. (**C**) Pyrrhotite-pentlandite sulfide-matrix breccia. Note sharp contact of breccia vein with host rock. (**D**) Sulfide-matrix breccia vein at Mikissoq (Drill core MQ13-29, 111.65 m). (**E**) Sulfide-matrix breccia at Mikissoq (drill core MQ13-29, 104.2 m). Width of drill core is 4.76 cm in each photograph

chalcopyrite-rich than in the remainder of the Ni belt, with broadly even proportions of pyrrhotite, chalcopyrite and pyrite (Fig. 5A-C).

Mineral compositions of the intrusions were determined by Waterton et al. (2020) and, for Spotty Hill South, in the present study. Orthopyroxene has Mg# 67–77 (up to 80 in melanorite) and Cr_2O_3 0.23%. Clinopyroxene has Mg# 79–85 (87 in melanorite) and Cr_2O_3 0.44 wt%. Plagioclase has An23-59, the lower values occurring mainly in retrogressed samples (Waterton et al. 2020). Mineral compositions at Spotty Hill South are slightly less evolved than in the remainder of the belt, with orthopyroxene having Mg# 75–81 (up to 84 in olivine rich sample OC48) and Cr_2O_3 0.23 wt%, clinopyroxene having Mg# 0.82–0.88 and Cr_2O_3 0.55 wt% (Mg#87–90 and Cr_2O_3 up to 0.84% in OC48), and plagioclase being mostly of composition An 27–43, with

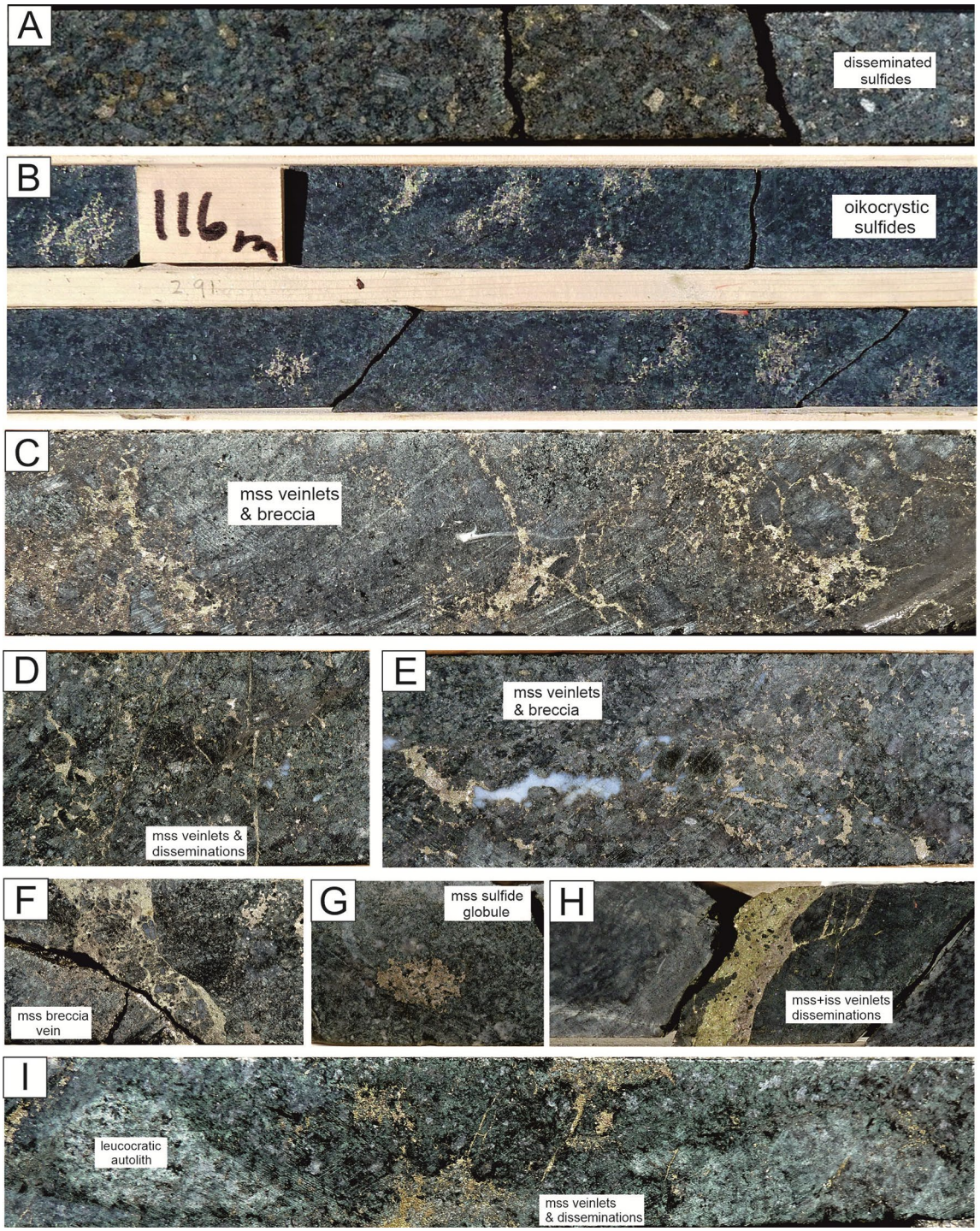

Fig. 3 (**A**) Disseminated (interstitial) sulfides at Spotty Hill, drill core MQ12-005, 106.5 m. Sample has 7500 ppm Ni, 1400 ppm Cu, 200 ppb PGE, and 13ppb Au. (**B**) Patchy disseminated sulfides from Imiak Hill, drill core MQ13-28, 116 m. Sample has 2380 ppm Ni, 560 ppm Cu, 125 ppm Co, 3.5 ppb PGE + Au. (**C**) Veinlets and disseminations of mainly pyrrhotite and pentlandite, Spotty Hill, drill core MQ12-005, 146.7 m. (**D** + **E**) Sulfide veinlets of predominantly Po and Pn at Fossilik, drill core MQ13-18, 115.1 m. Note sulfide and quartz filling same vein in E. (**F**) Sulfide matrix breccia vein of pyrrhotite and pentlandite, Fossilik, drill core MQ13-18, 51.80 m. (**G**) Sulfide globule of pyrrhotite and pentlandite, Centre target, drill core MQ13-32, 64 m. (**H**) Composite chalcopyrite-pyrrhotite sulfide vein in gneiss, Imiak Hill, drill core MQ13-28, 210 m. (**I**) Leucocratic autoliths hosted in mineralized gabbronorite with sulfide disseminations and fracture-hosted veinlets, Centre target, drill core MQ13-32, 71.3 m. Width of drill core is 4.76 cm in each photograph

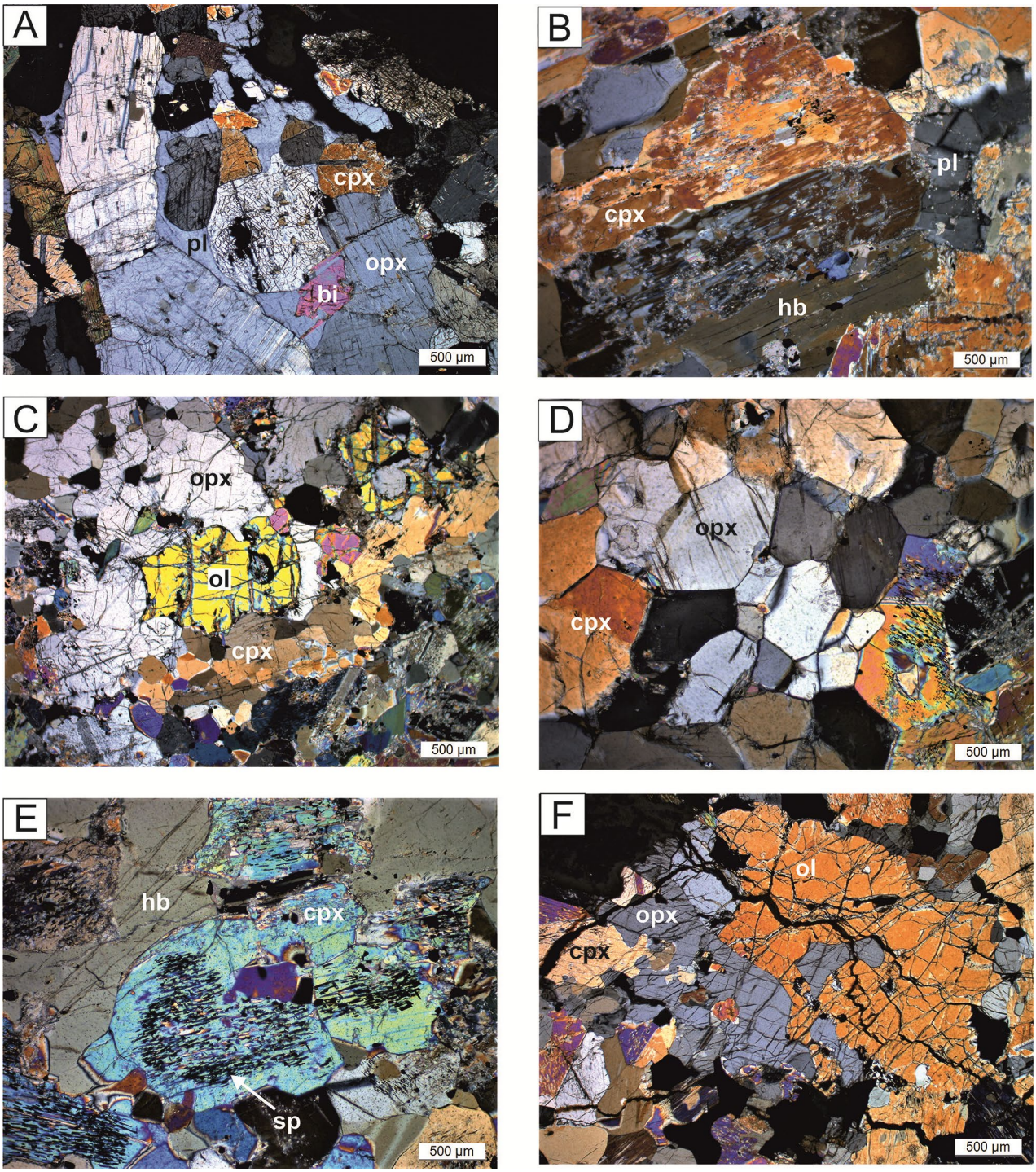

Fig. 4 Petrography of samples from Spotty Hill South intrusion. (a) Melagabbronorite. Note subhedral pyroxenes and interstitial plagioclase, sample OC2, (b) Websterite. Note beginning amphibolitisation of pyroxene, and highly equilibrated plagioclase textures, sample OC11, (c-e) Lherzolite-websterite, note locally highly equilibrated textures with 120° triple junctions. In e, clinopyroxene contains abundant exsolution of spinel. Sample OC34, (f) Lherzolite, sample OC48.

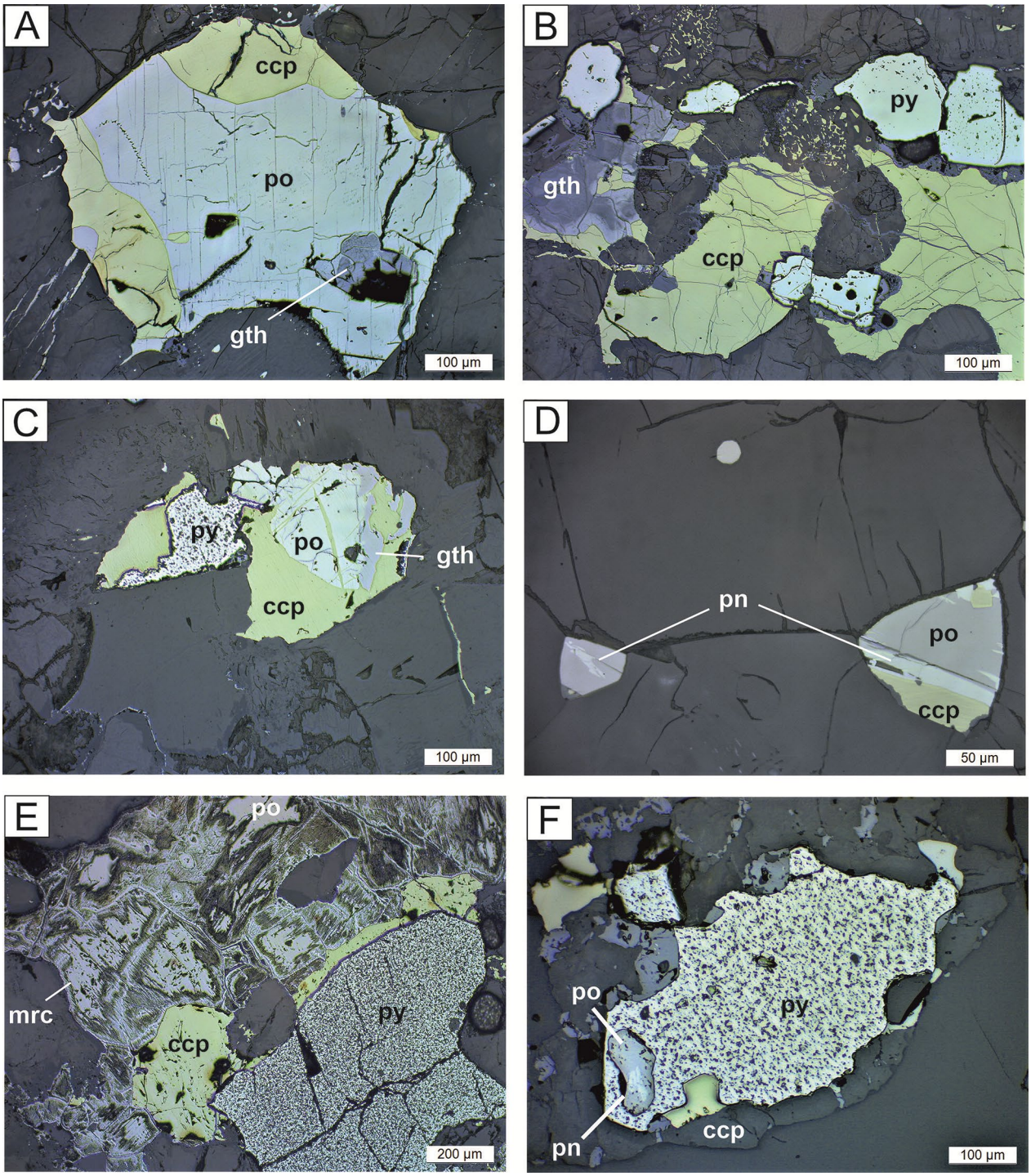

Fig. 5 Reflected light microscopy of samples from Spotty Hill South intrusion. (**a**) Bleb-like grain of chalcopyrite (ccp) and pyrrhotite (po), with grey area next to cavity (bottom right) being goethite (gth, FeOOH), sample OC43. (**b**) Chalcopyrite-pyrite (py) assemblage, with pyrrhotite being replaced by goethite. Note incipient "bird's eye" development, sample OC43. (**c**) Pyrrhotite-chalcopyrite-pyrite, with pyrrhotite beginning to be replaced by goethite. Sample OC11. (**d**) Small grains of po-ccp, with pyrrhotite showing exsolution flames of pn. Note equilibrium textures with well-developed 120° dihedral angles, sample OC34. (**e**) Pyrite, ccp and po, the latter partially replaced by marcasite (mrc) and possibly py, paragneiss from Taqisak, sample D1614. (**f**) Paragneiss, note small exsolution lamellae of pentlandite in pyrrhotite

some nearly pure albite also occurring. The olivine in the Spotty Hill South ultramafic body (sample OC43) has Fo 83–86 and NiO 0.24–0.38%.

Chemical maps

Selected samples from four intrusions in the Imiak Complex, comprising the Mikissoq, Spotty Hill, Spotty Hill South and Imiak Hill bodies, as well as Target P-053 have been chemically mapped using FEG-SEM and are described in more detail below. Phase areas (modal %) have been calculated from principal component analysis "Phase Area" function built into Aztec 6.0. Note that there are significant "unassigned" pixels in all maps. These mostly constitute cracks, holes and grain boundaries between phases where two mineral compositions are combined in one spectrum.

Drill core MQ16-113, 234.5 m, Mikissoq

The main silicate minerals are orthopyroxene (69 mod.%), clinopyroxene (12 mod.%), plagioclase (2 mod.%) and minor amphibole (0.7 mod.%), establishing the rock as a websterite. Clinopyroxene forms large (up to ~ 1 cm) oikocrysts enclosing subhedral chadacrysts of orthopyroxene. The oikocrysts are largely free of plagioclase and sulfides and are surrounded by domains of sulfide-poor orthopyroxene. Plagioclase forms interstitial crystals between subhedral orthopyroxene. No zonation could be detected in any of the silicate minerals. Sulfides make up ~ 20 mod.% of the rock. Relatively coarse sulfide grains form an interconnected network across the slide, separated by silicate domains that contain rare and small grains of sulfide. The modal proportions of the sulfides are pyrrhotite (10 mod.%), pentlandite (2 mod.%), pentlandite-pyrrhotite intergrowth (4.75 mod.%), as well as minor pyrite (0.43 mod.%) and traces of chalcopyrite (< 0.1 mod.%). Pyrrhotite forms intergrowths with pentlandite and is locally replaced by a Ca-rich phase. Pentlandite is partially replaced by fine pyrite. Chalcopyrite forms fine disseminations in silicates.

Drill core MQ16-113, 236.8 m, Mikissoq

The micro textures in this sample (ESM 3 A) show many similarities to those of sample MQ16-113, 234.5 m. The main silicate minerals are orthopyroxene (~ 60 mod.%) and clinopyroxene (14.3 mod.%), rendering the rock a websterite. Orthopyroxene forms a network of subhedral and anhedral crystals as well as inclusions in clinopyroxene. Clinopyroxene forms large (up to ~ 1 cm) oikocrysts. Plagioclase is a minor phase (1.7 mod.%) forming interstitial crystals between the orthopyroxenes. Amphibole constitutes 0.4 mod.%. The clinopyroxene oikocrysts are surrounded by halos of orthopyroxene. Both the oikocrysts and the halos are free of sulfides (Fig. 6A). Sulfides comprise pyrrhotite (7.6 mod.%), pentlandite (9.3 mod.%) and pyrite (0.9 mod.%). The sample is almost free of chalcopyrite (0.14 mod.%). Silicate-sulfide mixtures make up 5.9 mod.%. Pyrrhotite and pentlandite are intergrown, forming a net-textured framework. Pyrite typically replaces pentlandite. Pyrrhotite forms veinlets and trails of very small grains infiltrating the silicate minerals, in contrast to the previous sample which showed little sulfide veining and contained significantly less pyrite.

Drill core MQ12-005, 119.4 m, Spotty Hill

The main silicate minerals of the rock are orthopyroxene (65 mod.%), plagioclase (9.5 mod.%) and clinopyroxene (6.4 mod.%), constituting a melanorite. Orthopyroxene forms euhedral and subhedral crystals of highly variable size, and small chadacrysts within oikocrysts of clinopyroxene and plagioclase. In addition to oikocrysts, plagioclase and clinopyroxene also form interstitial minerals. Plagioclase is normally zoned, with relatively calcic cores. The rock contains minor biotite (~ 1 mod.%) and trace apatite (< 0.1 mod.%). Sulfides make up ~ 20 mod.% of the rock, forming an interconnected network between the silicate minerals, constituting a classic net-texture (Fig. 6C). Pyrrhotite is the most common sulfide (12 mod.%), followed by pentlandite (4.7 mod.%). Pyrite forms very small grains (< 0.1 mod.%) locally replacing pentlandite. Chalcopyrite forms rare interstitial grains and veinlets (< 0.1 mod.%) which is reflected by the relatively high Ni/Cu ratio (~ 20) of the rock.

Drill core MQ14-66, 161.7 m, target P-013 (Spotty Hill)

The silicate minerals consist predominantly of clinopyroxene (~ 25–30 mod.%), plagioclase (13.2 mod.%), orthopyroxene (~ 15 mod.%) in the form of oikocrysts and intergrown with clinopyroxene, and amphibole (9.5 mod.%) replacing clinopyroxene. The rock is thus a gabbronorite. There are a few grains of serpentine within one of the plagioclase oikocrysts. The serpentine is mantled by orthopyroxene and possibly formed through alteration of olivine. Plagioclase forms large (up to > 1 cm), subhedral oikocrysts enclosing subhedral to anhedral chadacrysts (typically 1–2 mm) of mainly clinopyroxene and orthopyroxene (ESM 3B). Clinopyroxene within plagioclase oikocrysts is more calcic than clinopyroxene outside the oikocrysts. There are several grains of small (< 1 mm) apatite. Sulfides make up ~ 30 mod.% of the rock (Fig. 6D). They form an interstitial network between the silicate minerals. The sulfides consist mainly of pyrrhotite and pentlandite (16.6 and 5.6 mod.%, respectively, with an additional 8 mod.% representing

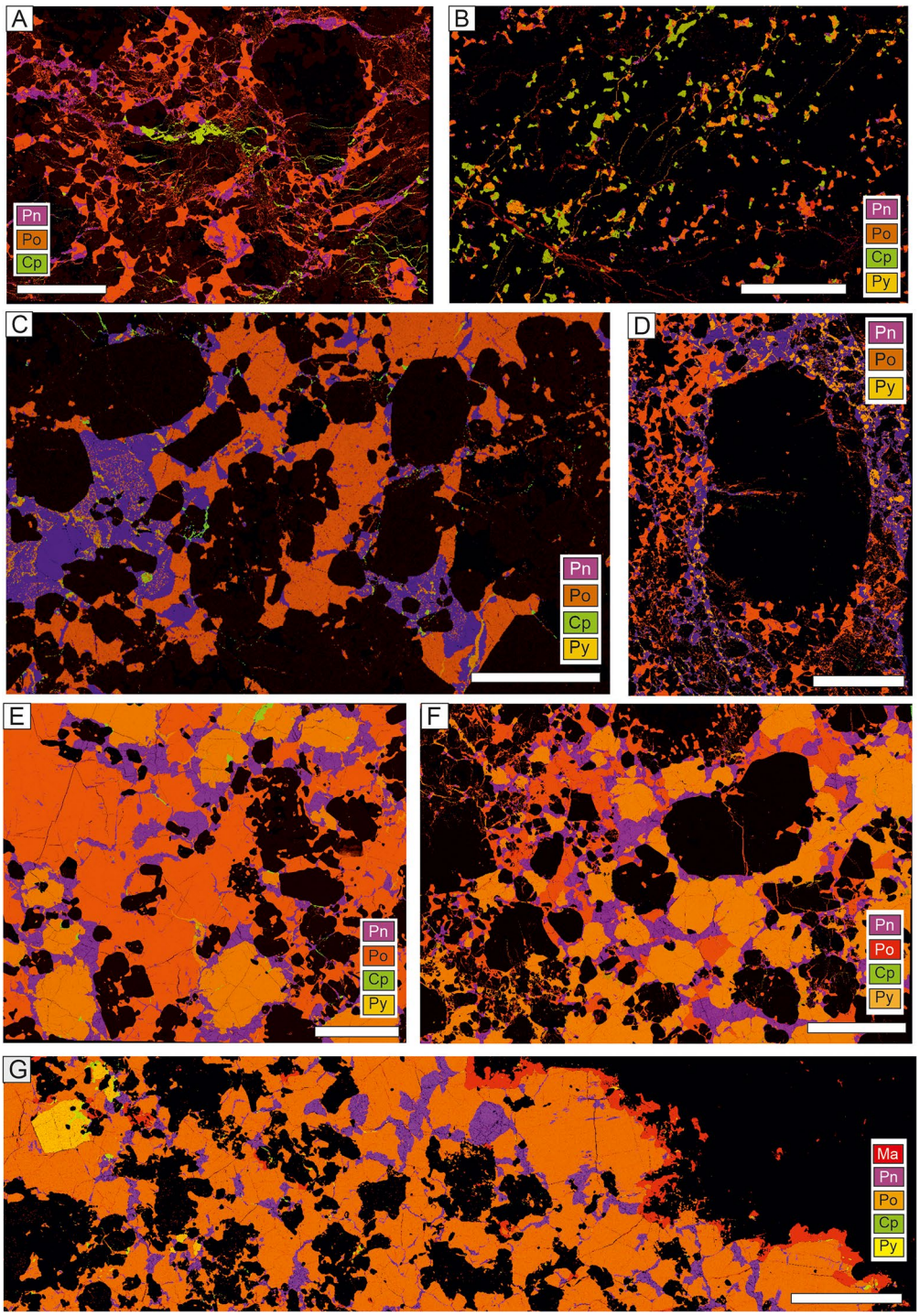

Fig. 6 Element maps of sulfide minerals in selected samples. (**A**) MQ16-113, 236.8 m, Mikissoq; (**B**) OC48, Spotty Hill South; (**C**) MQ12-005, 119.4 m, Spotty Hill; (**D**) MQ14-66, 161.7 m, Target P-01, note sulfide free nature of oikocryst. (**E**) MQ12-001, 16 m, Imiak Hill; (**F**) MQ12-001, 17 m, Imiak Hill; (**G**) MQ15-82, 110 m, Target P-053. Black colour denotes silicates. Scale Bar = 0.5 cm. Note sulfide poor nature of most silicates. Pn = pentlandite, Po = pyrrhotite, Cp = chalcopyrite, Py = pyrite, Ma = magnetite

mixtures between the two phases). There is almost no chalcopyrite (< 0.1 mod.%). Pyrite (0.9 mod.%) is always intergrown with pentlandite, but never with pyrrhotite. Notably, the plagioclase oikocrysts are essentially free of sulfides, apart from minor veinlets (Fig. 6D). This is analogous to the observations on oikocrysts from Mikissoq (ESM 3 A).

Drill core MQ15-82, 110 m, target P-053

The silicate minerals consist mostly of clinopyroxene (~ 20–25 mod.%) and amphibole (~ 15 mod.%), with minor orthopyroxene (~ 1–2 mod.%), biotite (~ 1 mod.%), plagioclase (~ 1 mod.%) and some calcite veins. The silicate portion of the rock is thus a hornblende-clinopyroxenite (ESM 3 C). Rare apatite grains can be up to 1 mm in size. There are several magnetite grains and a selvage of magnetite along the contact between the sulfidic intrusive and the host granite-gneiss (Fig. 6G). The magnetite selvage is distinctly zoned, with grains becoming less Cr rich towards (and within) the gneiss. The Si-map (not shown) indicates a subtle enrichment in very fine grained quartz in the mafic intrusive, within ~ 2 cm from the contact with the host gneiss. The sulfides form semi- massive aggregates, making up ~ 60 mod.% of the rock (Fig. 6G). They consist of pyrrhotite (~ 50 mod.%), pentlandite (~ 6 mod.%) and pyrite (~ 4 mod.%), the latter forming several large euhedral grains. Pentlandite forms networks and rims around pyrrhotite. There is very little chalcopyrite (~ 1 mod.%), mainly forming rims around pyrite. The gneissic host rock is essentially free of sulfide, consisting of quartz (~ 20–30 mod.%), alkali feldspar (~ 20–30 mod.%), normally zoned plagioclase (~ 40 mod.%), and biotite (~ 10 mod.%). Minor amounts of magnetite are mainly associated with biotite which is relatively enriched in Mg near the contact with the intrusive.

Drill core MQ15-82, 114.75 m, target P-053

The main silicate minerals of the rock are clinopyroxene (33.6 mod.%), plagioclase (12.2 mod.%), amphibole (6.2 mod.%) and orthopyroxene (4.2 mod.%)(ESM 3D). The silicate portion of the rock is thus a melagabbronorite. Clinopyroxene and orthopyroxene form subhedral crystals up to 0.5 cm in size. Clinopyroxene is usually rimmed by orthopyroxene and contains subhedral orthopyroxene inclusions. Plagioclase forms oikocrysts up to ~ 1 cm in size that typically have calcic cores and sodic rims. Apatite is more common than in the other samples, forming grains up to ~ 0.5 mm in size. The sulfides form a net-textured assemblage making up ~ 40 mod.% of the rock. Pyrite (16 mod.%) and pyrrhotite (20.5 mod.%) make up the bulk of the sulfides, with 3.4 mod.% pentlandite, 0.4 mod.% chalcopyrite and 2.6 mod.% pyrrhotite-pentlandite intergrowth. Chalcopyrite typically occurs along the margins of pyrite. As in most other samples, the silicates are essentially free of sulfides.

Drill core MQ12-001, 17 m, Imiak Hill

The main silicates are subhedral grains of orthopyroxene (45.4 mod.%, up to ~ 5 mm in size), with minor intercumulus plagioclase (1.2 mod.%) and small oikocrysts and interstitial grains of clinopyroxene (4 mod.%)(ESM 3E). The rock is thus an orthopyroxenite. The sulfides make up ~ 45 mod.% of the rock, forming the net-textured matrix to the silicates (Fig. 6F). The main sulfide minerals are pyrite (23 mod.%), pyrrhotite (16.4 mod.%, commonly forming thin veins within and along the edges of silicate minerals) and pentlandite (6.4 mod.%). There is very little chalcopyrite (0.3 mod.%). Note that Ni and Cu contents of the rocks are quite variable on a local scale, with assays of adjacent drill core samples showing 6.58% Ni + 3.75% Cu and 6.6% Ni + 0.9% Cu.

Drill core MQ12-001, 16 m, Imiak Hill

Silicates make up ~ 15 mod.% of the rock, mainly consisting of subhedral orthopyroxene (14 mod.%). Minor silicates include tabular plagioclase (1 mod.%), amphibole (0.25 mod.%) and biotite (0.25 mod.%). Apatite is a trace phase. The silicate portion of the rock is thus an orthopyroxenite. The bulk of the rock consists of sulfides, namely pyrrhotite (63 mod.%), pyrite (13.3 mod.%) and pentlandite (7.8 mod.%), with traces of chalcopyrite (0.12 mod.%) along fractures within, and along the margins of, pyrite. Large pyrite grains tend to be rimmed by grains of pentlandite. The whole rock assay of the rock indicates 6.6% Ni and 0.9% Cu.

Grab sample QC48, Spotty Hill South

Silicates make up ~ 90–95 mod.% of the rock, mainly consisting of subhedral clinopyroxene (62 mod.%), as well as anhedral, but broadly equant grains of olivine (13 mod.%) that are typically rimmed by orthopyroxene (7.8 mod.%). In addition, there is 12.7 mod.% amphibole, replacing clinopyroxene and orthopyroxene (ESM 3 F). The rock is thus a wehrlite. Minor phases include apatite, ilmenite, magnetite, phlogopite and sphalerite. The sulfides form disseminations and, locally, net textures, consisting of pyrrhotite (2.4 mod.%) and pyrite (0.9 mod.%). Chalcopyrite (1.2 mod.%) is concentrated in a broad linear zone diagonally across the slide (Fig. 6B). Pentlandite makes up < 0.1 mod.%, forming grains associated with, and flame-like lamellae within,

pyrrhotite (Fig. 5D). Goethite and marcasite replacement of pyrrhotite is quite common (Fig. 5).

Whole rock geochemistry

Lithophile elements

The lithophile whole rock data (e.g. CaO and MgO contents, Fig. 7) are consistent with petrographic observations in that in most samples, orthopyroxene exceeds clinopyroxene in abundance, and plagioclase proportions vary between ~80% and ~10%. True norites appear to be less abundant than gabbronorites, except for Spotty Hill and P-061. Melanorite and melagabbronorite are largely confined to the Imiak Hill Complex and Fossilik, and leucogabbronorite to Imiak Hill, P-022, P-049, P-059 and the Centre target (Fig. 7B). There are very few true gabbros in the belt.

The available data provide no indication that any peridotite was sampled, confirming that such rocks are rare in the Ni belt. The only olivine-rich intrusion studied so far is the predominantly ultramafic Spotty Hill South body. Since the Spotty Hill North intrusion is the most magnesian amongst the analysed mafic intrusions, it appears that the Spotty Hill intrusive cluster is the least evolved so far studied in the belt (Fig. 7B).

Zirconium contents of the intrusions are mostly between 10 and 50 ppm, consistent with petrographic observations suggesting that the rocks are meso- or orthocumulates containing more than ~10% trapped liquid component. Multi-element variation plots of five of our samples analysed using high-precision ICP-MS at UQAC indicate fractionated trace element patterns, with variable LILE and LREE enrichment, and negative Nb-Ta anomalies (ESM 4). The patterns show good overlap with the data of Garde et al. (2010) and Waterton et al. (2020).

Chalcophile elements

Rocks containing > 2 wt% nickel are largely confined to the Imiak Hill Complex (Imiak Hill, Mikissoq, Spotty Hill). For this reason, the Imiak Hill complex has been the focus of exploration. Rocks with somewhat lower Ni contents (0.1-2 wt%) occur in many other bodies and targets in the belt. For example, surface grab samples at Quagssuk (P-049), 20 km to the NE of the Imiak Hill Complex, yielded up to 3.35 wt% Ni. Other high grade grab samples were collected at targets P-094, G-017 and P-136, whereas grab samples with > 0.1% Ni were collected from targets G-028, Pingo, P-142, P-141, P-034, P-132, G-011.

The assay data from most of the intrusions show well defined positive correlations between Ni and S (Fig. 8A, B) suggesting that the relative proportions of Ni-rich pentlandite and Ni-poor pyrrhotite and pyrite remain largely constant. The highest Ni tenors occur at Spotty Hill, Mikissoq, Fossilik, and the P-032 and Centre targets (ESM 5). Note that high Ni tenors are not confined to any specific rock type (Fig. 8C, D). However, there is a trend of massive (> 60% sulfide) and semi-massive sulfides (> 30% sulfide) having lower tenors (Ni/S 0.1–0.3, 4–10% Ni) than disseminated sulfides (Ni/S up to ~0.5, > 10% Ni)(ESM 6).

Copper contents of the analysed rocks are mostly significantly lower than Ni contents, usually at < 1 wt%. Almost all samples with > 1% Cu are from Imiak Hill (Fig. 9A). The correlation between Cu and S is mostly strong, with the exception of the semi-massive and massive sulfides, particularly at Imiak Hill, Spotty Hill and P-022 (Sibolik)

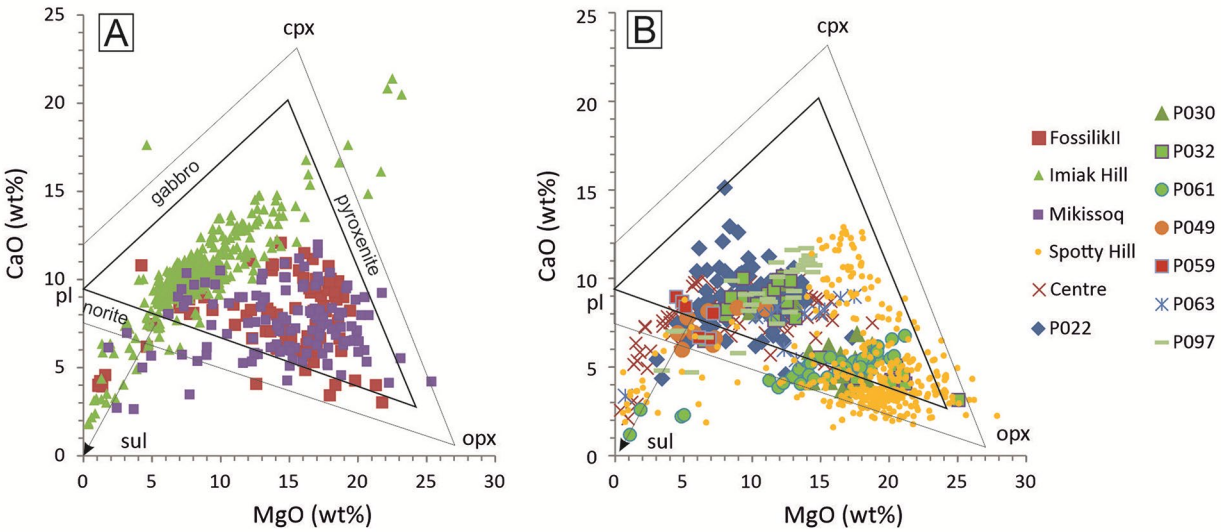

Fig. 7 Plot of CaO vs. MgO of sulfide-bearing intrusives. All data are normalised to sulfide free. Note that most bodies are gabbronoritic. Spotty Hill North appears to be the most orthopyroxene-rich locality

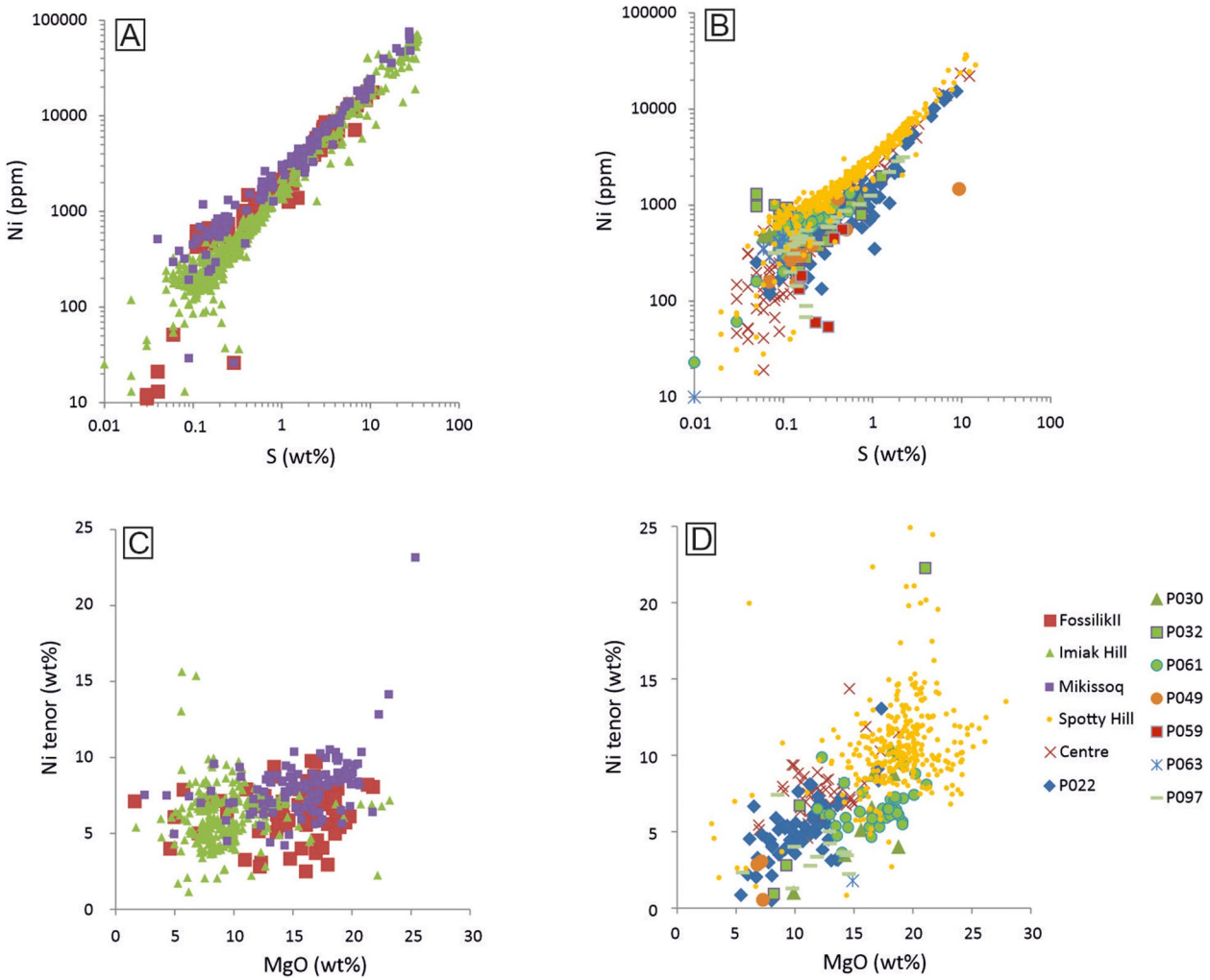

Fig. 8 Binary variation plots of **a, b** Ni vs. S, showing good positive correlation for all bodies. **c, d**: Ni tenor vs. MgO. All data are normalised to S free

which can be very Cu poor, containing largely pyrrhotite and pentlandite. Copper tenors of the rocks are highly variable, with a median value of 2.6 (ESM 7). Many of the highest Cu/S values occur at Mikissoq, Fossilik and P-013 (Centre target).

As a result of the relatively high Ni and low Cu contents in many of the rocks, Ni/Cu of the sulfides tends to be relatively high, typically ranging from 1 to 10, but with pronounced local variability (Fig. 9C, D). The median Ni/Cu in sulfide for the main deposits are: Spotty Hill 4.06, Centre 2.49, Imiak Hill 2.67, Mikissoq 2.33, and Fossilik 2.12. Note that there is no correlation between Ni/Cu and differentiation index Cr/V (Fig. 9C, D).

The distribution of Te, As, Bi, Sb and Se (TABS+) was assessed using the mantle-normalised diagram of Barnes and Mansur (2022) (Fig. 10A) wherein the TABS + as well as Cu, Pt and Pd are arranged in order of their partition coefficients into a sulfide liquid (Liu and Brenan 2015) to assess the effect of sulfide liquid segregation. Thorium and Nb were added to the plot to take into consideration the effect of crustal contamination. The average Th contents of our samples are 7.24 x PM, and Nb = 4.25 x PM, resulting in small negative Nb anomalies in the plot. The TABS patterns show a broadly flat trend from As (avg. 7.3 x PM) to Sb (14 x PM), followed by significantly higher values from Bi (101 x PM) through Cu (166 x PM) to Se (381 x PM) and Te (140 x PM), and variable concentrations of Pd (120 x PM) and Pt (46 x PM). The patterns resemble those of the Espedalen and Romsas Ni-deposits in Norway (Mansur et el. 2023a, b) which were explained by a model of monosulfide solid solution (MSS) fractionation. S/Se ratios are in the 7000 to 9000 range indicating that sedimentary S is present (Queffurus and Barnes 2015).

Compared to many other Ni-Cu sulfide deposits globally, the concentrations of the PGE in the Maniitsoq intrusions are relatively low. PGE contents are highest at Spotty Hill

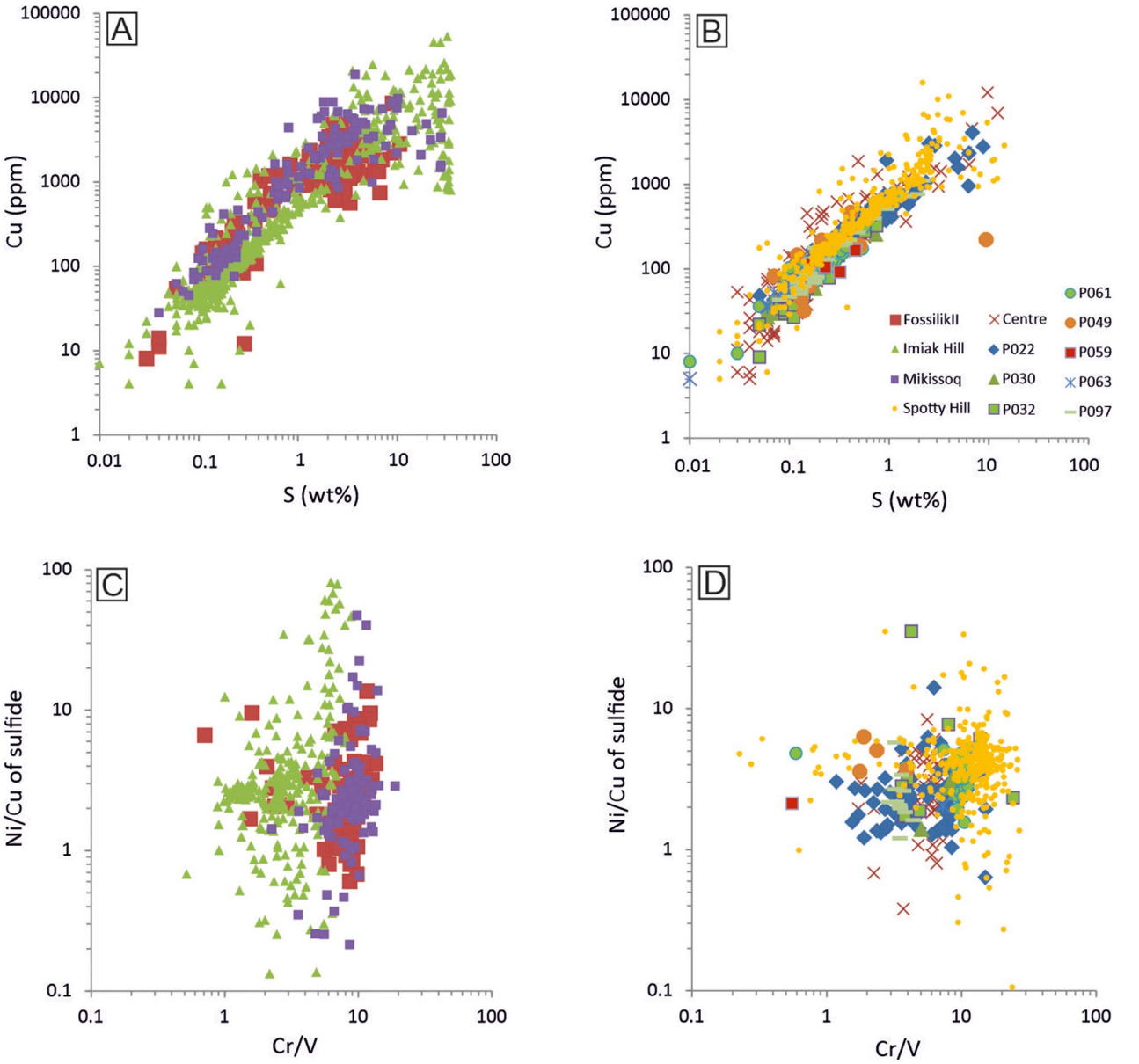

Fig. 9 **a, b**: Binary variation plots of Cu vs. S for analysed intrusions, showing generally good positive correlations, but high variation in semi-massive and massive sulfides, notably at Imiak Hill. **c, d**: Binary variation plots of Ni/Cu in sulfide vs. Cr/V of whole rocks, showing lack of fractionation control

North (reaching locally~1 ppm) and Fossilik (up to ~0.5 ppm). Most other intrusions have < 100 ppb PGE, with Imiak Hill being particularly PGE poor having PGE contents frequently below the detection limit of 2.5ppb for both Pt and Pd (Fig. 11a, b). PGE tenors of the Maniitsoq sulfides are mostly < 10 ppm. The highest tenors occur at the P-030 target and Spotty Hill North, whereas by far the lowest tenors occur at Imiak Hill. Correlations between PGE and S are generally positive and well defined within individual intrusions, but are poor for the belt as a whole, due to markedly different Pt + Pd/S ratios between intrusions (Fig. 11A, B).

Interestingly, relatively high PGE levels were found in some surface samples from across the belt. For example, in 2005, NunaMinerals A/S sampled a poorly exposed rusty zone in quartz-dioritic rocks about 350 m from KØ's Ikertup Kingingnera showing in the southern part of the project area. A composite sample yielded 0.36 ppm Pt, 1.74 ppm Pd, 0.17 ppm Au, 0.80% Ni, and 0.30% Cu. However, three boreholes (max. 237 m) intersected only weak mineralisation, with up to 143 ppb combined Pd and Pt and 0.20% Ni over 8 m. This suggests that the elevated PGE contents in the surface samples could reflect residual PGE enrichment due to weathering.

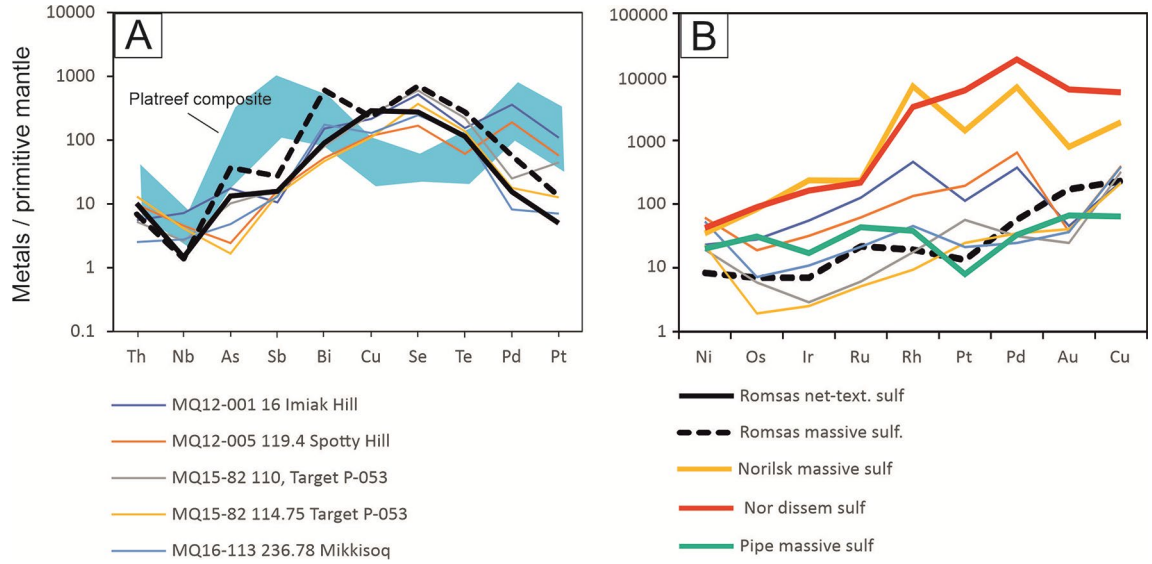

Fig. 10 (**a**) TABS patterns and (**b**) PGE + Ni + Cu + Au patterns of Maniitsoq samples. The average concentrations of Romsas massive and net-textured sulfides are shown as black lines (Mansur et al. 2023a)

Data for all 6 PGE using Ni sulfide fire assay are available for five of our drill core samples from four intrusions (Table 1; Fig. 10B). Because the selected samples are relatively sulfide rich, their PGE contents plot at the upper end of the compositional field for these intrusions (Fig. 11). The P-053 samples come from an intrusion for which no previous assays are available, and their PGE contents also are amongst the highest 10% analysed across the belt. Most notably, the analysis of a~20 g sample of semi-massive sulfide from Imiak Hill (MQ12-001, 17 m) yielded 2 ppm Pt + Pd and 1.3 ppm IPGE + Rh (a repeat analysis yielded essentially the same result). As the m-sized NAN assays for Imiak Hill all contain < 0.1 ppm PGE, this result indicates a strong nugget effect.

The metal patterns of three of the samples show a marked depletion in PGE (and Au) relative to Ni and Cu (Fig. 10B) and, apart from a positive Rh anomaly, a relatively flat general trend, with Pd/Ir between 2.5 and 23. The two samples from Imiak Hill and Spotty Hill are richer in all PGE, particularly Rh, Pt and Pd, showing somewhat more sloped trends. Pt/Pd of the samples are 0.55 to 3.3, with the PGE rich Imiak Hill sample having the lowest value (0.55). These Pt/Pd ratios broadly overlap with the range seen in the intrusions as a whole, which are typically between ~1 and 10 (Fig. 11E, F), higher than in most other global Ni-Cu sulfide deposits. Of the analysed intrusions, Spotty Hill and Target P-030 tend to have the lowest Pt/Pd, with averages at approximately unity.

Almost all intrusions studied have Cu/Pd far higher than the level of the primitive mantle (~7000, Fig. 11C, D), the main exception being target P-030 and a few samples from Spotty Hill and some other deposits. Note that even the most Cu-rich rocks which could possibly contain an intermediate solid solution (ISS) component are very PGE-poor (not shown).

Gold contents of the rocks reach up to ~300 ppb, with the highest values found in those intrusions that also show elevated PGE contents (Fossilik, Mikissoq, and Spotty Hill). The Centre target is also relatively Au rich, at ~60 ppb (Fig. 11G, H). Au/PGE ratios range between ~0.1 to ~1, with Spotty Hill showing the highest values. Most other Ni-Cu deposits typically have Au/Pt + Pd slightly above 0.1 (e.g., in Sudbury footwall ores and at Voisey's Bay and Jinchuan)(Naldrett 2004).

Variation in metal and S content with depth in intrusions

In most drill cores analysed there is no systematic variation with depth in S, Ni/Cu or Cr/V (ESM 8); In some drill cores, S increases with depth, whereas in other drill cores the trend is reversed.

Discussion

Tectonic setting and metamorphic history

Waterton et al. (2020) suggested that the intrusions of the Maniitsoq Ni belt were emplaced into an ultra-hot orogeny (Chardon et al. 2009) that formed in response to underthrusting of continental blocks and delamination of lithospheric mantle and mafic lower crust from the over-riding block. The delamination allowed the upwelling of hot, partially molten, depleted asthenospheric mantle followed by

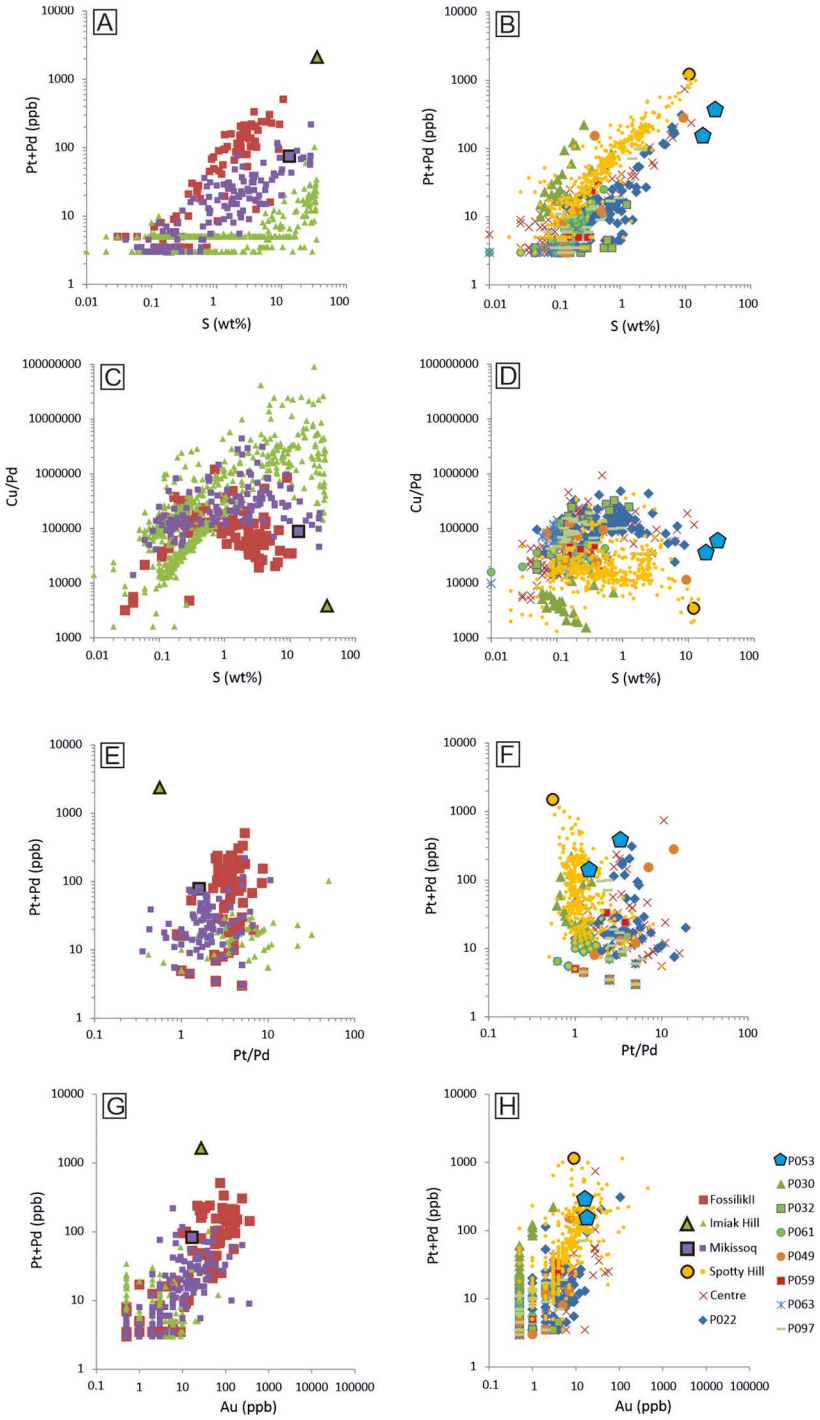

Fig. 11 **a**,**b**: Binary variation plots of Pt + Pd vs. S, showing positive correlations of PGE with S in individual intrusions, but with different trends between intrusions. **c, d** Binary variation plots of Cu/Pd vs. S showing that all bodies (apart from P-030) have Cu/Pd above the primitive mantle ratio, i.e., are PGE depleted. e, f: Pt + Pd vs. Pt/Pd. Note that most intrusions have Pt/Pd higher than unity, independent of PGE content. g, h: Binary variation plot of Pt + Pd vs. Au. See text for discussion

extensive partial melting of the mantle and invasion of the mantle melts into the crust producing the Maniitsoq mafic intrusives. The mantle upwelling resulted in high crustal temperatures providing a mechanism for melting of the mafic lower crust to produce the TTGs that are spatially closely associated with the nickeliferous mafic intrusives. The mafic and felsic magmas may have ascended along one of the major suture zones in the region, e.g., the Godthåbsfjord-Ameralik Belt.

Due to the combination of delamination, mechanical weakness, and thermal erosion, the orogenic crust (~30 km thick) and mantle lithosphere (~10 km thick) remained relatively thin, and modelled Moho temperatures were high (~900–1100 °C; Perchuk et al. 2018). Thus, following magmatism, the region underwent high-T / low-P granulite-facies metamorphism that commenced soon after the emplacement of the Maniitsoq mafic intrusives. The metamorphism with local anatexis overprinted primary igneous assemblages,

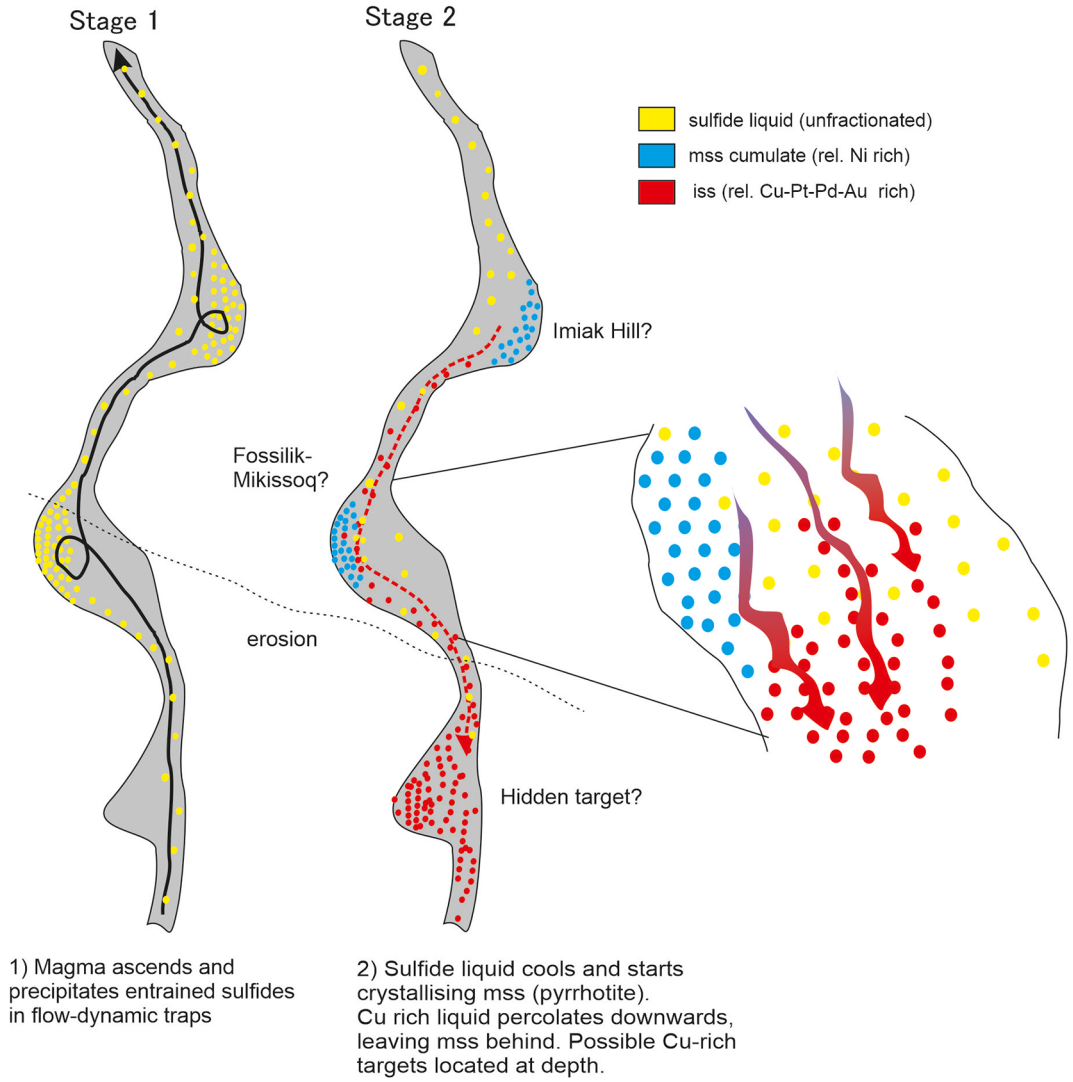

Fig. 12 Sketch model for origin of Maniitsoq intrusions. Step 1: Ascent and emplacement of basaltic magma entraining Ni-rich but PGE depleted sulfide melt. Step 2: Sulfide melt percolates downward through the conduits and fractionates to produce Ni-rich MSS, particularly in the upper portions of the conduits, and Cu-rich ISS, predominantly in the unexposed lower portions

causing reactions between plagioclase + orthopyroxene +/- melt to form clinopyroxene. The rocks then underwent pervasive hydration/retrogression at amphibolite facies, causing hydration of clinopyroxene and orthopyroxene to amphibole (Waterton et al. 2020; Yakymchuk et al. 2020).

The high crustal temperatures may have facilitated assimilation of the continental crust by the parent magmas to the nickel belt, as crustal temperatures must have been close to the melting point of the host TTGs for 10s of Myrs (Perchuk et al. 2018; Taylor et al. 2020; Yakymchuk et al. 2020). This model is consistent with recent suggestions that TTGs in the Maniitsoq region might be derived from relatively low pressure melting of mafic rocks (Yakymchuk et al. 2020), without requiring over-thickening or subduction of mafic crust (Laurent et al. 2020).

Shape and size of intrusions, and constraints on deformation

Detailed mapping by NAN geologists since 2011 showed that a large proportion of the Maniitsoq intrusions have lenticular, pod-like (e.g., Imiak Hill) or dyke-like shapes (e.g., targets P146 and 149) that typically follow the trend of the tectonic grain (Ravenelle and Weiershäuser 2017). The contacts of many intrusions with the gneissic host rocks are faulted. Some intrusions, e.g., Fossilik, show complex fold patterns at norite-orthogneiss contacts, interpreted to result from interference between F2 and F3 folds. Fossilik and other intrusions consist of several blocks, possibly resulting from tectonic dismemberment (ESM 9). Drilling and electromagnetic surveys showed that the sulfide mineralisation may be truncated and displaced by mylonite zones at depth,

Table 1 Composition of Maniitsoq samples analysed at UQAC

Drill core	MQ12-001 15	MQ12-05	MQ15-82	MQ15-82	MQ16-113 Mikisoq		mld
sample (m)	17	119.4	110	114.75	236.78	OC34	
Locality	Imiak Hill	Spotty Hill	P-053	P-053	Mikisoq	Spotty Hill S	
SiO2 (wt%)	14.8	36.81	16.2	27.53	35.37	51.34	0.04
TiO2	0.11	0.17	0.15	0.29	0.16	0.35	0
Al2O3	0.81	3.98	1.75	4.42	1.99	4.25	0.2
MgO	7.49	15.55	5.4	7.77	17.01	18.33	0.18
FeO						7.9	0.1
Fe*	35.13	20.01	35.81	26.10	20.76		0.07
MnO	0.07	0.14	0.09	0.1	0.14	0.16	0.03
CaO	0.75	2.63	3.59	7.34	4.15	15.58	0.75
Na2O	0.24	0.76	0.62	0.91	0.26	0.62	0.2
K2O	0.24	0.21	0.18	0.27	< mld	0.48	0.15
P2O5	< mld	0.02	0.04	0.07	< mld	< mld	0.01
S	34.68	10.67	28.63	18.57	12.03	na	0.001
Ni	4.4	3.6	3.03	2.32	3.55	0.06	0.001
Cu	0.54	0.29	0.64	0.28	0.32	0.01	0.002
Total	99.26	94.84	96.13	95.97	95.74	99.48	
Sc (ppm)	6.63	16.51	14.88	25.43	21.49	49.42	1.5
V	35	56	46	82	72	128.74	1
Cr	807	1318	473	754	1532	2722	10
Co	3290	913	1574	1079	685	68	1
Ni	43,979	35,970	30,302	23,237	35,457	558	10
Cu	5394	2931	6437	2788	3243	95	20
Zn	170	146	101	97	213	74	8
Ga	1.88	5.06	3.5	5.09	3.9	6.78	0.4
Rb	< dl	5.69	3.89	3.1	< mld	< mld	3
Sr	14	98	51	164	27	180	2
Y	0.92	2.6	2.99	6.48	2.21	12.8	0.08
Zr	8.38	15.08	11.8	25.5	6.1	35	3
Nb	3.29	2.1	1.21	1.91	1.28	1.27	0.4
Ba	47	97	70	121	45	282	3
La	0.97	3.56	3.56	8.81	1.2	20.4	0.1
Ce	2.61	7.46	7.75	20.3	2.91	53	0.1
Pr	0.34	0.96	1.05	2.61	0.48	7.23	0.2
Nd	1.2	3.54	4.71	11.1	2.06	32.4	0.17
Sm	0.23	0.79	0.71	1.93	0.65	6.73	0.12
Eu	< mld	0.21	0.25	0.52	0.14	1.5	0.08
Gd	0.26	0.67	0.87	1.9	0.53	4.95	0.19
Tb	< mld	0.1	0.1	0.22	0.09	0.55	0.04
Dy	< mld	< mld	0.53	1.17	< mld	2.89	0.5
Ho	< mld	0.14	0.11	0.25	0.12	0.49	0.1
Er	0.15	0.37	0.3	0.65	0.23	1.22	0.03
Tm	< mld	0.08	0.04	0.07	0.05	0.17	0.04
Yb	0.14	0.36	0.28	0.66	0.31	0.96	0.12
Lu	< mld	0.06	0.04	0.09	0.04	0.14	0.03
Hf	0.21	0.6	0.36	0.88	0.25	1.13	0.13
Pb	< mld	< mld	< mld	< mld	< mld	22.4	10
Th	0.35	0.62	0.33	0.82	0.16	1.78	0.05
U	0.07	0.14	0.07	0.14	0.06	0.3	0.03
Os (ppb)	92	19	15.9	3.35	8.14	0.84	0.09
Ir	170	30	7.3	4.15	11.6	0.59	0.05
Ru	613	92	24.2	13.2	35.7	3.86	0.08
Rh	398	36	12.7	4.33	13.7	0.72	0.19
Pt	720	379	296	84	46	2.85	0.31

Table 1 (continued)

Drill core	MQ12-001 15	MQ12-05	MQ15-82	MQ15-82	MQ16-113 Mikisoq		mld
sample (m)	17	119.4	110	114.75	236.78	OC34	
Locality	Imiak Hill	Spotty Hill	P-053	P-053	Mikisoq	Spotty Hill S	
Pd	1292	686	90	64	29	6.66	0.4
Au	38.6	9.6	17.3	18.2	10.7	3.2	0.52

mld=methods limit of detection

nd=not determined

*Fe all iron expressed as Fe in sulfide rich samples

e.g., at Imiak Hill. Thus, the combined field data imply that the original shape of the intrusions cannot be readily deduced or reconstructed.

Ravenelle and Weiershäuser (2017) draw comparisons between the Maniitsoq Ni belt and the sulfide-rich intrusive bodies in the Thompson Ni belt, which represent transposed, folded, and sheared fragments of komatiitic sills and flows, embedded within their sedimentary host rocks. However, we consider it unlikely that the Maniitsoq intrusives are fragments of one originally much larger, coherent komatiitic body that was dismembered during regional metamorphism. This is because (i) the individual intrusions have distinct compositions, notably in terms of PGE (Fig. 11A, B), (ii) there is little evidence in the belt for magmatic sulfides that are disconnected from mafic intrusives and instead hosted solely within the gneissic country rocks, with the exception of thin veins in some contact zones, and (iii) a komatiitic lineage is unlikely due to the scarcity of olivine. Based on their relatively small size yet locally high sulfide content, their irregular dyke-, pod- and sheet-like shapes, and the paucity of highly evolved rocks, the intrusions of the Maniitsoq Ni belt are instead interpreted to represent basaltic magma conduits (Fig. 12).

Generation and evolution of the parent magmas to the Maniitsoq intrusions

Based on the occurrence of enclaves of host rocks, hybridised contact zones, xenocrystic zircon cores, fractionated ITE patterns and ITE ratios resembling those of the gneissic host rocks, as well as enriched O, Nd and Hf isotopes relative to 3 Ga mantle, Waterton et al. (2020) argued that the intrusions of the Maniitsoq Ni belt crystallised from Mg-basaltic proto liquids (~13% MgO) that were contaminated with ~20–30% crust during ascent and/or emplacement. The contamination model is consistent with the relatively high S/Se of 7000–9000 in our samples. Based on broadly constant La/Nb at evolving Mg# (Waterton et al. 2020 and current data) and the S-poor nature of most regionally occurring crustal rocks, the bulk of contamination likely occurred prior to magma fractionation and final emplacement. The only sulfidic crustal rocks intersected so far in the belt are paragneisses of uncertain age which locally contain abundant lenses and veins of pyrite and pyrrhotite (Fig. 5E, F).

If the model of crustal contamination of the parent magma to the intrusions is correct, the relatively unenriched Nd and Hf isotopic data of the intrusions (εHf values −1.1 to 0.0, εNd 0 to +2.4) would require that the original magma had strongly depleted Nd and Hf isotopes. Waterton et al. (2020) argued that the parent magmas were sourced from ancient (>3.8 Ga) depleted mantle because no amount of crustal contamination of a hypothetical parent melt derived from a primitive mantle-like source can match the average trace element and Hf isotope characteristics of the Maniitsoq intrusives. A depleted mantle source is also consistent with primitive mantle normalised Nb<Ti≈HREEs and high Al_2O_3/TiO_2 ratios calculated for the intrusives (corrected for plagioclase fractionation, Waterton et al. 2020).

The parent magma to the Maniitsoq intrusives could potentially be represented by fine grained mafic marginal rocks of the Imiak Hill intrusion intersected in several drill cores. The rocks have Al-basaltic compositions with approximately 6.7% MgO, 17.3% Al_2O_3, 9.8% CaO, 5.4% Fe_2O_3, 0.23% TiO_2, 0.13% S, 134 ppm Cr, 54 ppm Zr, 51 ppm Cu and PGE contents mostly below the detection limit of 2.5 ppb. However, the rocks have relatively high Ni (avg. 190 ppm) compared to many other basalts with ~7% MgO which typically contain significantly less than 200 ppm Ni. For example, Bushveld B2 Al-tholeiite has ~120 ppm Ni (Barnes et al. 2010), and the average Ni content of MORB is 92 ppm (Gale et al. 2013). Possibly, the fine grained marginal rocks were infiltrated by sulfides. Alternatively, the rocks could contain a small amount of sulfides digested during magma ascent and emplacement, consistent with the positive correlation between MgO and Ni (ESM 11).

Origin of the sulfide mineralisation

General considerations

Key features of the Maniitsoq sulfide mineralisation that need to be consistent with any petrogenetic model include the following: (i) The composition of the sulfides, comprising mainly pyrrhotite, pentlandite, and chalcopyrite is

typical of magmatic sulfide mineralisation. (ii) The mean composition of the sulfides is relatively "unevolved", with Ni/Cu averaging ~ 3, Ni tenors reaching 14%, and Pd/Ir 3–22 (avg 10); (iii) Individual sulfidic samples show a wide range in Ni/Cu, from 10 to 1, suggesting significant fractionation of sulfide melt prior to or after final emplacement; (iv) The mineralisation is relatively PGE poor, with typical PGE tenors of sulfides being < 10 ppm, and Cu/Pd above primitive mantle values; (v) Most sulfides have unusually high Pt/Pd (1–10) and Au/PGE (0.1->1). (vi) The sulfides have relatively high S/Se ratios (7000–9000), indicating the presence of significant crustal S (Queffurus and Barnes 2015). (vii) The sulfides show interstitial textures, and sulfide matrix breccias have knife sharp contacts with the mafic host rocks.

Normally, one might expect that relatively hot, vigorously convecting Archean mantle, overlain by relatively thin lithosphere, should facilitate relatively large degree melting of mantle plumes, dissolving all mantle sulfide and resulting in relatively PGE-rich magmas. For example, our MELTS modelling shows that at relatively low degrees (15%) of partial melting of primitive mantle, the partial melt is S undersaturated and the residual mantle is essentially barren of sulfide. However, as summarised above, the Maniitsoq intrusives are strongly PGE depleted. The most likely reason is that the magmas underwent contamination and sulfide segregation at high R factors (ratio of silicate melt to sulfide melt, Campbell and Naldrett 1979) prior to final emplacement. This caused precipitation of relatively small amounts of PGE-rich sulfides, whereas Ni and Cu contents of the magmas were not significantly depleted. During continued ascent and/or final emplacement the PGE-depleted magmas assimilated additional crustal sulfur triggering renewed sulfide melt saturation and segregation producing relatively Ni and Cu rich sulfides with low PGE contents and high S/Se ratios. Due to subsequent sulfide melt fractionation to be discussed below, we cannot constrain the original bulk composition of the sulfides, and hence the precise value of the R-factor.

Formation of sulfide matrix breccias

The key textural features of magmatic sulfide matrix breccias have been summarised by Barnes et al. (2016). The rocks typically have high, but variable sulfide contents (10–50 mod.%) and contain large oikocrysts barren of sulfides as well as numerous autoliths and fragments of the host rocks. The breccias tend to be closely associated with net textured, disseminated and blebby sulfides, as is observed at Maniitsoq (ESM 10).

Barnes et al. (2016) interpreted sulfide matrix breccias to be of non-tectonic origin, formed from hot, dense, low-viscosity sulfide melt that percolated downward through a crystal mush displacing interstitial silicate melt or low-melting solid silicates at infiltration-melting fronts. The authors suggested that the process is driven by a positive feed-back loop of percolating sulfide melt pushing away silicate liquid which allows more efficient wetting and better percolation. The longer the pathways get the more the sulfide melt veins grow, the only counteracting force being freezing of the sulfide melt. The percolating sulfides would cause cracks during infiltration of semi-solidified cumulates, facilitating further invasion. Barnes et al. (2016) provide examples from Nova, Sudbury, Savannah, Karaleakh, Voisey's Bay and Kambalda, with another example being the Flatreef of the Bushveld Complex (Maier et al. 2023). In some cases, e.g., at Savannah and Kalatongke, the sulfides are proposed to have percolated into the keel of chonoliths (Wei and Wang 2023; Barnes et al. 2016).

Sulfide-matrix breccias at Maniitsoq show many of the features described by Barnes et al. (2016), notably abundant autoliths and country rock fragments showing subordinate sulfide veins, and oikocrysts barren of sulfides. These allow to place constraints on the timing of sulfide mineralisation, suggesting that the sulfides formed after the formation of the oikocrysts. However, in contrast to many of the other deposits described in Barnes et al. (2016) the Maniitsoq sulfide-matrix breccias, as well as the disseminated sulfides and most sulfide veins, consist largely of pyrrhotite-pentlandite-pyrite. Chalcopyrite is relatively rare, hosted largely by thin veinlets.

We can think of two possible models to explain the relatively Cu-poor nature of the mineralisation: (i) The sulfide melt could have fractionated during downward percolation through the cumulates, with relatively dense ISS percolating relatively more efficiently to deeper levels of the crust (Fig. 12). The process could have been facilitated by magma emplacement into a hot, slowly cooling orogen. The model is consistent with the pronounced variation in Cu and Ni contents of the rocks (ESM 12), particularly at Imiak Hill (Fig. 9A). The latter locality also shows unusually high Au/PGE ratios, possibly reflecting incompatibility of Au with regard to ISS (Barnes and Ripley 2016). (ii) The alternative is that the sulfides underwent fractionation during peak metamorphic partial melting. Waterton et al. (2020) suggested peak metamorphic grades of 800 °C at Maniitsoq, and Helmy et al. showed that sulfide melt coexists with MSS until 700 °C. However, no indications of anatexis were observed in any of the norite belt rocks. The only leucomes found are in mafic granulites outside of the belt (Yakymchuk et al. 2020).

The low Pd/Pt of the sulfide mineralisation across the belt requires an additional process to sulfide melt fractionation because both Pt and Pd are incompatible with regard

to ISS. Palladium is normally considered to be more soluble than Pt in hydrothermal fluids (Hanley 2005; Sullivan et al. 2021), suggesting that Pd could have been mobilised during amphibolite facies metamorphism. This could also have caused the pronounced nugget effect found in sample MQ12-001, 17 m at Imiak Hill.

Origin of distinct composition of Spotty Hill intrusion

Sulfides in the Spotty Hill intrusion have somewhat higher Ni tenors (ESM 5), PGE contents (Fig. 11B) and Cr/V (Fig. 9) than those in the other intrusions studied. The relative proportion of orthopyroxene is also higher at Spotty Hill (Fig. 7B). The reasons for the elevated metal grades and tenors remain unclear. Sulfide compositions may be controlled by the Ni content of the parent magma which in turn may be controlled by the degree of partial mantle melting, fractionation state, contamination with crust, and variable R factors (mass ratio of sulfide melt to silicate melt) during sulfide segregation. The relatively high Cr/V ratios of the Spotty Hill silicates and Ni tenors of the sulfides could suggest that the parent magmas were somewhat less evolved than those from which the other intrusions crystallised.

Exploration implications

The data presented in the preceding sections, including the size and shape of the intrusions, the abundance of autoliths and country rock xenoliths, and the textural evidence for percolation of sulfide melt through the cumulates could suggest that the intrusions of the Maniitsoq Ni belt represent fossil magma conduits, now containing mafic cumulates with significant disseminated and locally massive sulfides. Magma conduits represent the highest priority target for magmatic sulfides globally (Naldrett 1999; Li and Naldrett 1999; Maier et al. 2001; Barnes et al. 2016). The relatively Ni rich composition of the sulfides, interpreted to result from highly efficient sulfide melt fractionation could suggest that the exposed intrusions of the Ni belt represent the upper portions of magma conduits and that there is potential for Cu-rich sulfides in unexposed deeper portions of the belt (Fig. 12). As none of the drill cores shows a systematic trend of Cu enrichment with depth, the postulated percolation process appears to have been extremely efficient.

Conclusions

The ~3.01 Ga Maniitsoq Ni-Cu sulfide deposits of western Greenland represent some of the oldest magmatic ore deposits on Earth. The mineralisation occurs in the form of disseminated, net-textured and massive sulfides, as well as sulfide matrix breccia veins, hosted in poorly layered, predominantly gabbronoritic intrusions, with less abundant norite, pyroxenite, and peridotite. The country rocks are granite gneiss. The bodies are relatively small, at a few 100s to a few 1000 m in cross section. Due to locally pronounced tectonism, their original sizes remain poorly defined. Assay data from more than 2000 samples indicate relatively high Ni/Cu (~3 on average) and low PGE contents. This is interpreted to reflect the predominance of MSS cumulate formed via sulfide melt fractionation and percolation during emplacement. Because most bodies have distinct compositions, we consider it unlikely that they are tectonised fragments of an originally much larger intrusion. Instead, the combined data suggest that they could be magma conduits.

The general association of the most Ni-rich sulfides globally with Archean komatiites could suggest that Archean magmatic ore formation processes are fundamentally different than in post-Archean environments. However, the present study provides no support for this hypothesis as the Maniitsoq Ni deposits have textural and compositional features that resemble those from post-Archean deposits.

Supplementary Information The online version contains supplementary material available at https://doi.org/10.1007/s00126-024-01282-3.

Acknowledgements We thank Premium Nickel Resources Ltd for granting permission to publish the data. Peter Lightfoot assisted in sample collection and Tony Oldroyd is thanked for producing the thin sections.

Funding Some of this work was co-funded by the European Union and UK Research and Innovation (SEMACRET, 101057741). WDM conceived the project and collected the samples. DD Muir and SJB conducted the analyses and provided input to discussions and data interpretations. KS provided input to discussions and data interpretation.

References

Allaart JH, Friend CRL, Hall RP, Jensen SB, Roberts IWN (1978) Continued 1: 500 000 reconnaissance mapping in the Precambrian of the Sukkertoppen region, southern West Greenland. Rapport Grønlands Geologiske Undersøgelse 90:50–54

Barnes S-J, Mansur ET (2022) Distribution of Te, as, Bi, Sb, and Se in mid-ocean ridge basalt and komatiites and in picrites and basalts from large igneous provinces: implications for the formation of magmatic Ni-Cu-platinum group element deposits. Econ Geol 117(8):1919–1933

Barnes S-J, Ripley EM (2016) Highly siderophile and strongly chalcophile elements in magmatic ore deposits. Rev Mineral Geochem 81(1):725–774

Barnes S-J, Maier WD, Curl EA (2010) Composition of the marginal rocks and sills of the Rustenburg Layered Suite, Bushveld Complex, South Africa: implications for the formation of the platinum-group element deposits. Econ Geol 105(8):1491–1511

Barnes SJ, Cruden AR, Arndt N, Saumur BM (2016) The mineral system approach applied to magmatic Ni–Cu–PGE sulphide deposits. Ore Geol Rev 76:296–316

Bédard LP, Savard D, Barnes S-J (2008) Total sulfur concentration in geological reference materials by elemental infrared analyser. Geostand Geoanal Res 32:203–208

Burden S (2014) The conduit-hosted sulphide deposits in the Maniitsoq region of Southwest Greenland. BSc dissertation, Cardiff University, 51 p

Campbell IH, Naldrett AJ (1979) The influence of silicate: sulfide ratios on the geochemistry of magmatic sulfides. Econ Geol 74:1503–1506

Chardon D, Gapais D, Cagnard F (2009) Flow of ultra-hot orogens: a view from the precambrian, clues for the Phanerozoic. Tectonophysics 477:105–118. https://doi.org/10.1016/j.tecto.2009.03.008

Duncalf F (2014) Exploration and Assessment of Ni-Cu sulphide deposits within the Greenland Norite Belt, Maniitsoq South West Greenland. BSc dissertation, Cardiff University

Gale A, Dalton CA, Langmuir CH, Su Y, Schilling J-G (2013) The mean composition of ocean ridge basalts. Geochem Geophys Geosy 14:489–518. https://doi.org/10.1029/2012gc004334

Garde AA, Pattison J, Kokfelt TF, Mcdonald I, Secher K (2013) The norite belt in the Mesoarchaean Maniitsoq structure, southern West Greenland: conduit-type Ni-Cu mineralisation in impact-triggered, mantle-derived intrusions? Geol. Surv Den Greenl Bull 28:45–48. https://doi.org/10.34194/geusb.v28.4722

Garde AA, Dyck B, Esbensen KH, Johansson L, Möller C (2014) The Finnefjeld domain, Maniitsoq structure, West Greenland: Differential rheological features and mechanical homogenisation in response to impacting? vol 255. Precambrian Research, pp 791–808

Hanley JJ (2005) The aqueous geochemistry of the platinum-group elements (PGE) in surfcial, low-T hydrothermal and high-T magmatic-hydrothermal environments. Explor Platinum-Group Elem Deposits 35:35–56

Heaman LM (2014) Report on U-Pb MC-ICPMS Zircon Dating of North American Nickel Gabbro Samples. Internal report for prepared for North American Nickel Inc

Laurent O, Björnsen J, Wotzlaw J-F, Bretscher S, Pimenta Silva M, Moyen J-F (2020) Earth's earliest granitoids are crystal-rich magma reservoirs tapped by silicic eruptions. Nat Geosci 13:163–169. https://doi.org/10.1038/s41561-019-0520-6

Li C, Naldrett AJ (1999) Geology and petrology of the Voisey's Bay intrusion: reaction of olivine with sulfide and silicate liquids. Lithos 47(1–2):1–31

Linnebjerg B (2019) A petrographic study of Ni-sulfide mineralization in the Maniitsoq region of SW Greenland, BSc dissertation, University of Copenhagen, 75p

Liu Y, Brenan J (2015) Partitioning of platinum-group elements (PGE) and chalcogens (Se, Te, as, Sb, Bi) between monosulfide-solid solution (MSS), intermediate solid solution (ISS) and sulfide liquid at controlled fO2–fS2 conditions. Geochim Cosmochim Acta 159:139–161

Maier WD, Li C, De Waal SA (2001) Why are there no major Ni–Cu sulfide deposits in large layered mafic-ultramafic intrusions? Can Mineral 39(2):547–556

Maier WD, Barnes SJ, Godel BM, Grobler D, Smith WD (2023) Petrogenesis of thick, high-grade PGE mineralisation in the Flatreef, northern Bushveld Complex. Mineralium Deposita, pp.1–22

Mansur ET, Slagstad T, Dare SA, Sandstad JS (2023) Geology and sulphide geochemistry of the Ni-Cu-Co mineralisation of the Espedalen Complex, Norway: constraints for the distribution of magmatic sulphides within a variably deformed anorthosite suite. Ore Geology Reviews, p 105666

Mansur ET, Sandstad JS, Slagstad T, Miranda ACR, Dare SA, Nilsson LP (2023a) Geology, sulphide geochemistry and geochronology of the Romsås Ni-Cu-Co mineralisation, Norway: Implications for ore formation and regional prospectivity. Lithos, p.107244

Marker M, Garde AA (1988) Border relations between the amphibolite facies Finnefjeld Gneiss complex and granulite facies grey gneisses in the Fiskefjord area, southern West Greenland. Rapport Grønlands Geologiske Undersøgelse 140:49–54

Naldrett AJ (1999) World-Class Ni-Cu-PGE deposits: key factors in their genesis, vol 34. Mineralium deposita, pp 227–240

Naldrett AJ (2004) Magmatic sulfide deposits: geology, geochemistry and exploration. Springer Science & Business Media

Nielsen BL (1976) Economic minerals. In Escher, A. & Watt, W. S. (edit.). Geology of Greenland, 460–487. Copenhagen: Geo! Surv. Greenland

Nutman AP, Hagiya H, Maruyama S (1995) SHRIMP U-Pb single zircon geochronology of a Proterozoic mafic dyke, Isukasia, southern West Greenland. Bull Geol Soc Den 42:17–22

Olierook HK, Kirkland CL, Hollis JA, Gardiner NJ, Yakymchuk C, Szilas K, Waterton P (2021) Regional Zircon U-Pb geochronology for the Maniitsoq region, southwest Greenland. Sci Data 8(1):139

Perchuk AL, Safonov OG, Smit CA, van Reenen DD, Zakharov VS, Gerya TV (2018) Precambrian ultra-hot orogenic factory: making and reworking of continental crust. Tectonophysics 746:572–586. 10.1016/j. tecto.2016.11.041

Queffurus M, Barnes S-J (2015) A review of sulfur to selenium ratios in magmatic nickel–copper and platinum-group element deposits. Ore Geol Rev 69:301–324

Ravenelle JF, Weiershaeuser L, Cole G (2017) Report No.: 3CN024.004. Updated Independent Technical Report for the Maniitsoq Nickel-CopperCobalt-PGM Project, Greenland. https://s1.q4cdn.com/725069486/files/doc_downloads/technical_reports/Technical_Report_2017, pdf (Accessed December 15, 2023)

Savard D, Barnes S-J, Meisel T (2010) Comparison between nickel-sulfur fire assay Te Co-precipitation and isotope dilution with high-pressure asher acid digestion for the determination of platinum-group elements, rhenium and gold. Geostand Geoanal Res 34:281–291

Secher K (1983) The Geological Survey of Greenland Report No, vol 115. Noritic rocks and associated nickel-copper-sulphide occurences in Sukkertoppen district, central West Greenland. Copenhagen, Denmark: Geological Survey of Denmark and Greenland Bulletin, p 23

Sullivan NA, Zajacz Z, Brenan JM, Tsay A (2021) The solubility of platinum in magmatic brines: insights into the mobility of PGE in ore-forming environments. Geochim Cosmochim Acta 316:253–327

Taylor RJM, Johnson TE, Clark C, Harrison RJ (2020) Persistence of meltbearing Archean lower crust for > 200 m.y.-an example from the Lewisian complex, northwest Scotland. Geology 48:221–225. https://doi.org/10.1130/g46834.1

Waterton P, Hyde WR, Tusch J, Hollis JA, Kirkland CL, Kinney C, Yakymchuk C, Gardiner NJ, Zakharov D, Olierook HK, Lightfoot

PC (2020) Geodynamic implications of synchronous norite and TTG formation in the 3 Ga Maniitsoq Norite Belt, West Greenland. Frontiers in Earth Science, 8, p.562062

Wei B, Wang J (2023) Percolation of sulfide liquid through semi-consolidated silicate cumulates: textural evidence from breccia ores in the Kalatongke Cu-Ni sulfide deposit, NW China. J Asian Earth Sci 253:p105706

Windley BF, Garde AA (2009) Arc-generated blocks with crustal sections in the North Atlantic craton of West Greenland: crustal growth in the Archean with modern analogues. Earth Sci Rev 93(1–2):1–30

Yakymchuk C, Kirkland CL, Hollis JA, Kendrick J, Gardiner NJ, Szilas K (2020) Mesoarchean partial melting of mafic crust and tonalite production during high-T–low-P stagnant tectonism, Akia Terrane, West Greenland. Precambrian Res 339:p105615